

# Inferring Earthquake Source Properties From Laboratory Observations and the Scope of Lab Contributions to Source Physics

N. M. Beeler

*US Geological Survey, Menlo Park, California, USA*

I summarize implications of lab-measured high slip speed fault strength for earthquake source properties as could be inferred from radiated displacements. Source physics influence the radiated field through the magnitude of dissipative processes that reduce the energy available to be radiated. Based on the energy budget I conclude, as others have previously, that the static stress drop and a measure of efficiency, the ratio of apparent stress to static stress drop, are particularly useful for classifying source physics. For the limited laboratory experiments on known mechanisms of high speed strength loss, low temperature friction, flash weakening, bulk melting, and unexpected weakening associated with silica gel formation, I estimate the implied stress drop and efficiency, with reference to typical (MPa stress drops, 20% efficiency). Conventional friction produces typical stress drops and typical efficiencies, thus it can naturally explain source properties of typical earthquakes. Unexpected weakening produces large stress drops and typical efficiencies. This is not a likely mechanism to produce typical earthquakes but could be involved in exceptional events. Flash weakening produces high efficiency and is not a likely mechanism for producing typical earthquake source properties. Dynamic stress drops would be very large and on-fault effective shear fracture energies are negligible. Similar to flash weakening, bulk melting will produce large dynamic stress drops. Not enough is known at present to estimate efficiency; the on-fault effective shear fracture energy is relatively small.

## 1. INTRODUCTION

Seismically radiated energy is responsible for the damaging ground motions that lead to loss of life and property during an earthquake. While recorded waveforms carry virtually all the available spatial and temporal information from an earthquake source, measurement and physical interpretation of the radiated field are controversial. Interpretations of seismic radiation are

especially equivocal with regard to whether source physics and the ratio of radiated energy to seismic moment change with earthquake magnitude. These are central motivating topics of 2005 Chapman conference and of this special volume.

Select recent seismological data indicate that the stress measure of radiated energy  $\tau_a$  (the apparent stress), proportional to the ratio of radiated energy to seismic moment, increases with earthquake size [e.g., *Mayeda and Walter, 1996; Kanamori et al., 1993*]. Since it is generally accepted that static stress drop ( $\Delta\tau$ ) is independent of moment and that typical earthquake stress drops are a few MPa [*Aki, 1967; Hanks, 1977*], apparent stress increasing with moment requires that large earthquakes are more efficient [e.g., *Kanamori and Heaton, 2000*],

Earthquakes: Radiated Energy and the Physics of Faulting  
Geophysical Monograph Series 170  
This paper is not subject to U.S. copyright.  
Published in 2006 by the American Geophysical Union.  
10.1029/170GM12

radiating more energy per area per slip than small events. As co-seismic total slip increases with seismic moment, the amount of shear-induced heat increases and co-seismic source temperatures are extremely high for the largest earthquakes [McKenzie and Brune, 1972; Sibson, 1975]. So, one interpretation of scale-dependent apparent stress is that it reflects a reduction in dynamic strength due to shear heating [Kanamori and Heaton, 2000].

However, observations of increasing apparent stress with moment are not definitive [Ide and Beroza, 2001; Ide et al., 2002]. Rather than evidence of changes in source physics, Ide and Beroza [2001] and Ide et al. [2002] believe that trends, at least in some studies, are artifacts due to measurement or analysis errors associated with estimating radiated energy. Bandwidth limitations can lead to underestimates, particularly for small earthquakes [Ide and Beroza, 2001] that often have corner frequencies of the same order as the maximum observable frequency. For such earthquakes, to determine apparent stress, some of the radiated energy must be estimated otherwise an artificial size dependence can arise. Other arguments against size scaling of apparent stress are presented by Ide et al. [2002]. By independently determining site and path effects and a frequency dependent attenuation, Ide et al. [2002] find Long Valley borehole-recorded earthquakes, previously thought to show size dependence, have stress drop and apparent stress that do not vary systematically with seismic moment.

In addition to questions about the validity of the observations, because seismic data contain limited indirect information about the source, scale-dependent apparent stress by itself cannot be easily interpreted as evidence of changes in source physics. Source physics influence the radiated field through the magnitude of dissipative processes, for instance heat and latent heat, that reduce the energy available to be radiated. No doubt the source is a three dimensional volume in which dissipative and inelastic processes operate (dilatancy, melting, other phase changes, thermal expansion of pore fluid, hydrofracture, creation of fracture surface energy, etc); only outside the source is rock predominantly elastic and able to transmit information unambiguously. Since earthquake seismology involves interpretation of elastodynamic waves, the wavefield contains only indirect information about source processes. And interpretations of the wavefield in terms of source physics can only be made in the context of particular source models. Many seismologically-inferred source parameters such as static and dynamic stress drop, fault area, fracture energy and measures of efficiency are model-dependent interpretations of seismic data rather than independent information. So, to determine source properties, scaling of these properties with earthquake size, and to infer the source physics that gives rise to the radiated field requires contributions from disciplines out-

side of seismology, particularly field geology, theory, numerical modeling, and experimental rock physics.

In this paper I review implications of laboratory rock mechanics experiments for earthquake source properties. A variety of processes that may affect fault strength or limit radiated energy during rapid slip have been identified. The goal of laboratory investigations is to access the particular process of interest, perform tests sufficient to characterize it and the associated intrinsic time and length scales and dependence on conditions (stress state, temperature, etc), such that constitutive relations can be constructed for use in models. To put lab work in context I'll initially discuss the energy budget of the seismic source, measures of earthquake efficiency and how they may relate to dissipation within the source region. I identify necessary fault properties to be measured for use in models and data analysis. Then I summarize the existing data from mechanisms of high speed strength loss, conventional low temperature friction [e.g. Byerlee, 1978], flash melting [Goldsby and Tullis, unpublished], bulk melting [Hirose and Shimamoto, 2005] and unexpected weakening due to gel formation [Goldsby and Tullis, 2002]. The implications of lab data for seismically measurable quantities are discussed. Large differences in spatial and temporal scale, slip, slip speed, stress, and temperature between earthquakes and laboratory tests, raise questions about the relevance of lab measures to earthquake source physics. I try to objectively define limits of applicability of lab data to understanding the earthquake source.

## 2. THE EARTHQUAKE ENERGY BUDGET

The total energy released during an earthquake is  $E_T = \bar{\tau} M_o / \mu$  where  $\bar{\tau}$  is the spatially-averaged shear stress in the direction of shear offset,  $\mu$  is the shear modulus and  $M_o$  is the seismic moment. Ignoring gravitational and rotational terms the total energy  $E_T$  is partitioned between radiated energy  $E_R$ , and the sum of energy that is dissipated or stored within the source by frictional heating, fracture and other processes. An often used source representation is as heat  $E_F$  and 'fracture energy'  $E_G$

$$E_T = E_R + E_F + E_G. \quad (1)$$

$E_G$  in (1) is related to concepts from both classic fracture mechanics and laboratory observations.

The idea of fracture energy comes originally from the Griffith energy balance for tensile crack propagation [Griffith, 1920]. For a crack to propagate, the energy release rate, the total energy per unit area of crack advance, must exceed the energy dissipated or stored as the crack advances. The critical energy release rate  $G_c$ , so defined when the

energy released equals the energy adsorbed, is thus the energy associated with inelastic breakdown processes of the material at the crack tip. In the case of a purely tensile crack,  $G_c$  can be equated with a material constant, the specific surface energy (the surface energy per unit area)  $\Gamma$  of the fractured material,  $G_c = 2\Gamma/\Delta A$ , where  $\Delta A$  is the increment of surface area that is created as the crack advances. Were this fracture surface energy the only contributor to  $E_G$  in (1), then  $E_G = G_c A$ . Instead, through consideration of rock physical properties it is well known that  $E_G \neq G_c A$  for earthquakes [Ida, 1973; Andrews, 1976; Rice, 1980; Wong, 1986].

Room temperature laboratory observations from soil [Palmer and Rice, 1973], fault [Okubo and Dieterich, 1981; 1984], and rock mechanics [Byerlee, 1970; Wong, 1982] indicate that fault strength during failure can be represented as a gradual loss of strength with slip  $\delta$  from a yield or peak strength  $\tau_p$  to a residual strength  $\tau_f$  (Figure 1). This 'slip weakening' defines an energy per area associated with strength loss, in excess of the residual strength

$$G_e = \int_0^s \tau_k d\delta - \tau_f s, \quad (2)$$

where  $s$  is total slip and  $\tau_k$  is the slip-dependent fault strength [Rice, 1980]. Slip-weakening has long been used in models of the seismic source [Ida, 1972] and in spontaneous dynamic earthquake rupture models [Andrews, 1976].

An important extension of Griffith [1920] is the dynamic shear analogue of fracture surface energy, namely, that during rupture propagation there must be energy dissipated or stored in excess of the heat generated by slip on the fault surface [Ida, 1972; Andrews, 1976]. This excess energy arises because as a rupture nucleates and propagates there are high stresses preceding the rupture front that increase in amplitude and spatial extent with distance of propagation. Because real materials have finite yield strength, the high stress associated with the propagating rupture must

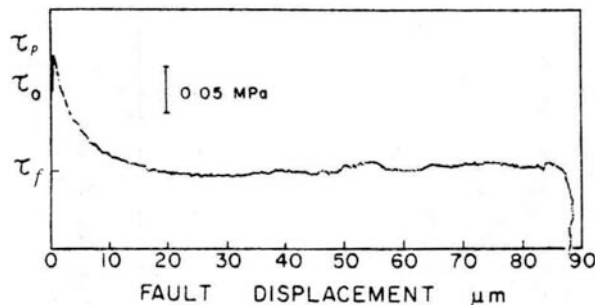


**Figure 1.** Slip-weakening during dynamic rupture propagation on a pre-existing fault between nominally flat surfaces of Sierra granite at 2.76 MPa normal stress [Okubo and Dieterich, 1984].

induce yielding or fracture which dissipate energy. Thus, there is an earthquake effective shear fracture energy that is analogous to the both the Griffith criteria and lab observations of slip weakening, though the energy adsorption mechanism and spatial extent are not specified without consideration of a particular material strength relationship [Andrews, 1976; 2005].

### 2.1 The Simplified Representation of Source Energy

A common, idealized representation of the earthquake energy budget [e.g., Kanamori and Heaton, 2000; Chester *et al.*, 2005] based on simple slip-weakening is shown in Figure 2. The total energy can rarely be deduced from the radiated wavefield because single event recordings contain no information on the ambient stress [e.g., Brune, 1970; Randall, 1972]. The dependence on ambient stress is handled by using the spatially-averaged initial  $\tau_0$  and final  $\tau_f$  stresses, related to  $\bar{\tau}$  by  $\bar{\tau} = (\tau_0 + \tau_f)/2$ , and the static stress drop,  $\Delta\tau = \tau_0 - \tau_f$ . The stress measure of radiated energy is the apparent stress  $\tau_a = \mu E_R/M_0$ . In Figures 2 and 3 various energies released per unit rupture area (Joules/m<sup>2</sup>) are depicted as regions of stress versus slip (Pa m). In this particular view of energy (Figure 2), fault yield strength is assumed equal to the initial stress and drops gradually with slip to a residual strength. The residual strength is assumed to be equivalent to the final stress [Rowan, 1960]. This simple model allows the terms in (1) to be defined in terms of the static stress drop and apparent stress. Since the stress drops from the yield strength exactly to the residual strength, all the energy available from the static stress drop is in excess of the heat  $E_p$ , and heat can be eliminated from the balance and happily ignored altogether. So, the energy associated with the stress drop is exactly partitioned between radiated and fracture energy, allowing the simple definition of fracture energy,

$$E_G = \left( \frac{\Delta\tau}{2} - \tau_a \right) As. \quad (3)$$

(3) has been used with seismological observations recently to infer changes in fracture energy and other source properties with event size by Abercrombie and Rice [2005]. Also (3) allows a longstanding measure of partitioning between radiated and 'available' energy, the radiation efficiency, to be defined simply as  $\eta_r = E_R/(E_R + E_G)$  [Husseini and Randall, 1976; Husseini, 1977], or

$$\eta_r = \frac{2\tau_a}{\Delta\tau}. \quad (4)$$

Using the model (3), the efficiency of earthquakes of various size and different tectonic settings are easily categorized [Venkataraman and Kanamori, 2004].

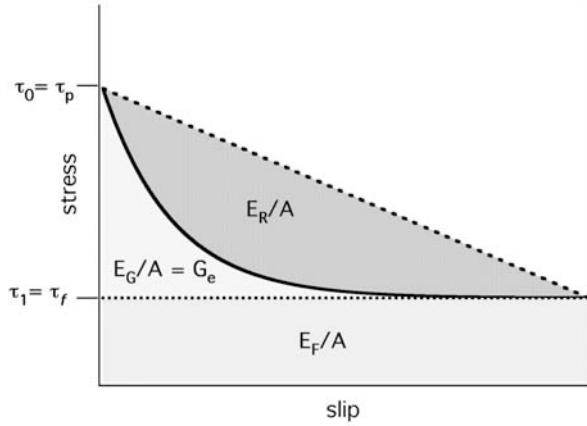


**Figure 2.** Simplified representation of source energy partitioning (3) between heat  $E_F$  (medium), fracture energy  $E_G$  (light) and radiated energy  $E_R$  (dark), based on a slip-weakening relation, no strength excess, and Orowan's assumption [Kanamori and Heaton, 2000].  $\eta_r=0.71$  (4) and  $\eta_{sw}=0.357$  (7).

However, there are simplifications of the earthquake source inherent in Figure 2 and equation (3) that are not consistent with seismic observations, existing source models, laboratory data and theory, as follows. As mentioned above, as an earthquake rupture propagates there is high concentrated stress in front of the rupture. Outside the nucleation zone, rupture can be initiated at a yield strength that exceeds the initial stress  $\tau_0$  [Andrews, 1976], and dynamic stress drops  $\Delta\tau_d = \tau_p - \tau_f$  are not consistent with the model (3) depicted in Figure 2. The difference between the yield strength and initial stress, the “strength excess”  $\tau_p - \tau_0$ , limits slip and rupture speeds [e.g., Andrews, 1985]. So, strength excess is an important consideration, though seismologic observations may not constraint it [Guatterri and Spudich, 2000].

Orowan's assumption that rupture ceases when the final stress equals the residual strength is also not consistent with many commonly used earthquake source models, models of self-healing slip pulses, or with laboratory observations. For rupture propagation in lab tests, the final stress is generally lower than fault strength [e.g., McGarr, 1994], both for confined and unconfined ruptures. This is stress ‘overshoot’ due to inertia, propagation and arrest. Overshoot, defined formally below, is observed in numerical simulations of arrested rupture where propagation is an expanding crack [see Kostrov and Das, 1988, p 189-191, and references therein]. Furthermore, it is expected that the final stress is greater than the average shear strength (undershoot) when rupture propagates as a self-healing slip pulse [Heaton, 1990]. So, while loss of fault strength (slip weakening) allows earthquakes to nucleate and propagate, to under-

stand arrest and energy partitioning it is necessary consider fault strength that may be higher than the initial stress [also see Cocco *et al.*, this volume] and following slip weakening may subsequently increase or further decrease with velocity, slip or time.

An additional concern is attributing types of energy (heat, surface energy) to the specific regions in Figure 2. As discussed in more detail in section 3, in laboratory experiments [Okubo and Dieterich, 1981; 1984; Wong, 1982; 1986] ‘fracture energy’ is heat rather than fracture surface energy. Similarly, in the recent theoretical calculations of slip weakening due to pore fluid pressurization by Rice [2006] and in models of dynamic rupture allowing off-fault yielding [Andrews, 1976; 2005], the dissipated energy during strength loss is heat rather than surface energy [also see Cocco *et al.*, this volume]. Conversely, a portion of energy attributed to heat in Figure 2 is true fracture surface energy, as brittle shear always causes some comminution. For example, aseismic slip at moderate normal stress (25–100 MPa) over a few hundred mm produces a large percentage of material so comminuted that it is amorphous to electron diffraction, requiring that the particles are <10 nanometers in size [Yund *et al.*, 1990]. For earthquakes this comminution generated fracture surface energy may be a significant contribution [e.g., Wilson *et al.*, 2005]. If most of the coseismic slip occurs following strength loss, much of the coseismically generated surface energy from wear is from sliding at the residual strength.

## 2.2 Model-independent Representation of Source Energy

So, the simple source model (3) (Figure 2) does not describe the range of possible strength and slip behaviors at high velocity or the partitioning between heat and latent energy sinks. Instead of (1), partition energy as

$$E_T = E_R + E_k \quad (5a)$$

Taking dissipated energy to be  $E_k = \bar{\tau}_k M_o / \mu$  and expressing in terms of stress we have

$$\bar{\tau} = \bar{\tau}_k + \tau_a \quad (5b)$$

$\bar{\tau}_k$  is the stress measure of energy dissipated and stored in the source, spatially- and slip-averaged over the entire source region. It is a representative ‘strength’ of the fault, and is so designated throughout this paper, acknowledging it represents energy distributed within the source, both on-fault and off-fault energy, including heat and surface energy. Also, abandon ad-hoc assumptions of  $\tau_0 = \tau_p$  and  $\tau_f = \tau_1$ . Rearranging (5), the apparent stress can be written in terms

of static stress drop and stress overshoot  $\xi = (\bar{\tau}_k - \tau_1) / \Delta\tau$  [McGarr, 1999] as

$$\tau_a = \Delta\tau(0.5 - \xi). \quad (6)$$

Apparent stress cannot be negative, so overshoot is bounded to be  $<1/2$ . Overshoot measures the average dynamic strength  $\bar{\tau}_k$  relative to the residual stress  $\tau_1$ ; positive values reflect high dynamic strength relative to the stress level (Figure 3a) and low and negative values of  $\xi$  reflect low relative strength (Figure 3c), indicating enhanced dynamic weakening.

Costs of abandoning the simple source model (3) are that fracture energy and dynamic stress drop are not simply defined, and that  $E_f$  can't be separated from radiated or fracture energy. Still, (6) does not void recent results in source scaling of fracture energy [Abercrombie and Rice, 2005] and classification of large earthquake efficiency [Venkataraman and Kanamori, 2004]. As noted by Abercrombie and Rice [2005], their analysis of fracture energy does not require Orowan's assumption and can be conducted for any value of overshoot. For (5) radiation efficiency is undefined, however (5) specifies a more general measure of efficiency compatible with Venkataraman and Kanamori's, as follows.

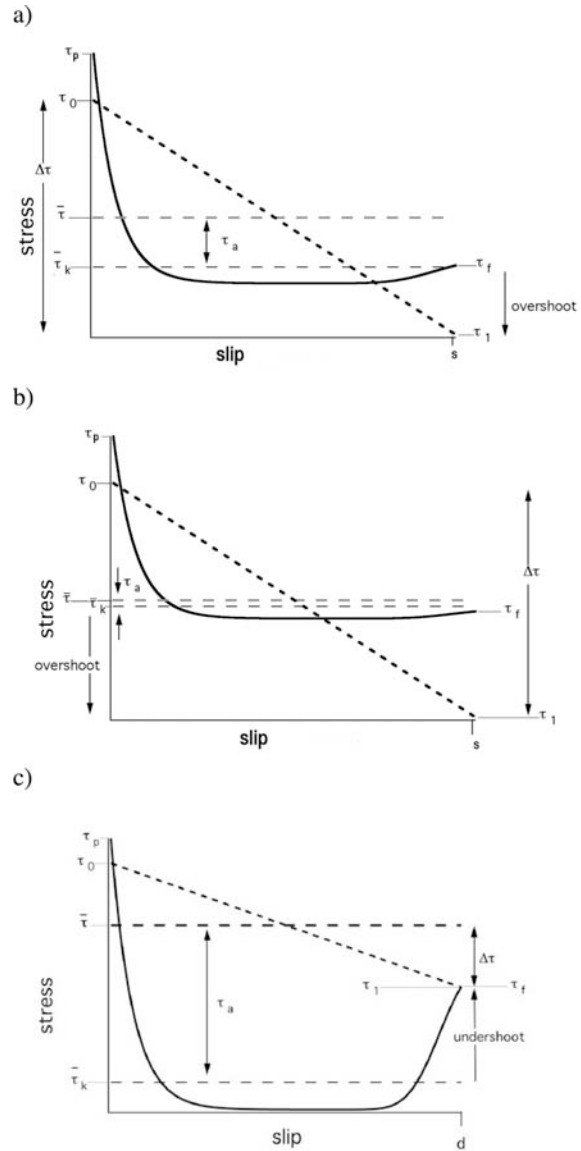
*2.21 Efficiency and overshoot.* Savage and Wood [1971] considered bounds on apparent stress relative to the static stress drop; their measure of efficiency follows naturally from (6)

$$\eta_{SW} = \frac{\tau_a}{\Delta\tau} = 0.5 - \xi. \quad (7)$$

Shaw [1998] and Beeler et al. [2003] refer to (7) as loudness and the Savage-Wood efficiency, respectively. The radia-

**Figure 3.** Block diagrams showing energy partitioning as energy per unit fault area (Joules/m<sup>2</sup>) released during an earthquake; the efficiencies correspond to particular earthquakes from the study by Venkataraman and Kanamori [2004] shown in Figure 4. The fault strength (heavy) is properly scaled but it is an example. Stress (heavy dashed) is also shown; the area beneath is the total energy released per unit fault area. In these 3 examples the static stress drop and strength excess are fixed while the apparent stress varies. a) Typical efficiency, M7.5 Kamchatka earthquake of 06/1993. The dynamic strength is similar to the mean stress and is larger than the final stress, overshoot is positive  $\xi=0.29$  and efficiency  $\eta_{SW}=0.21$  is consistent with lab stick-slip faulting and fracture. b) Low efficiency, M7.5 Peru earthquake of 02/1996. The average dynamic strength is nearly the same as the mean stress, overshoot is almost complete  $\xi=0.473$ , and efficiency is lower,  $\eta_{SW}=0.026$ , than in a). c) High efficiency, the 1992 Landers earthquake. There is undershoot  $\xi=-0.76$  and high efficiency  $\eta_{SW}=1.26$  as might be caused by shear melting or pore fluid pressurization with self-healing rupture.

tion efficiency is the percentage of *available energy* that is radiated [Husseni and Randall, 1976; Husseni, 1977]. Unless a model of available energy and source dissipation are assumed, the radiation efficiency cannot be estimated. Fortunately, the efficiency (7) is twice Venkataraman and Kanamori's model-specific definition of radiation efficiency (4). Figure 4a shows their summary estimates of large earthquake efficiency re-plotted using (7). Superimposed are qualitative, speculative boundaries that separate the range of source energy partitioning. Some examples that



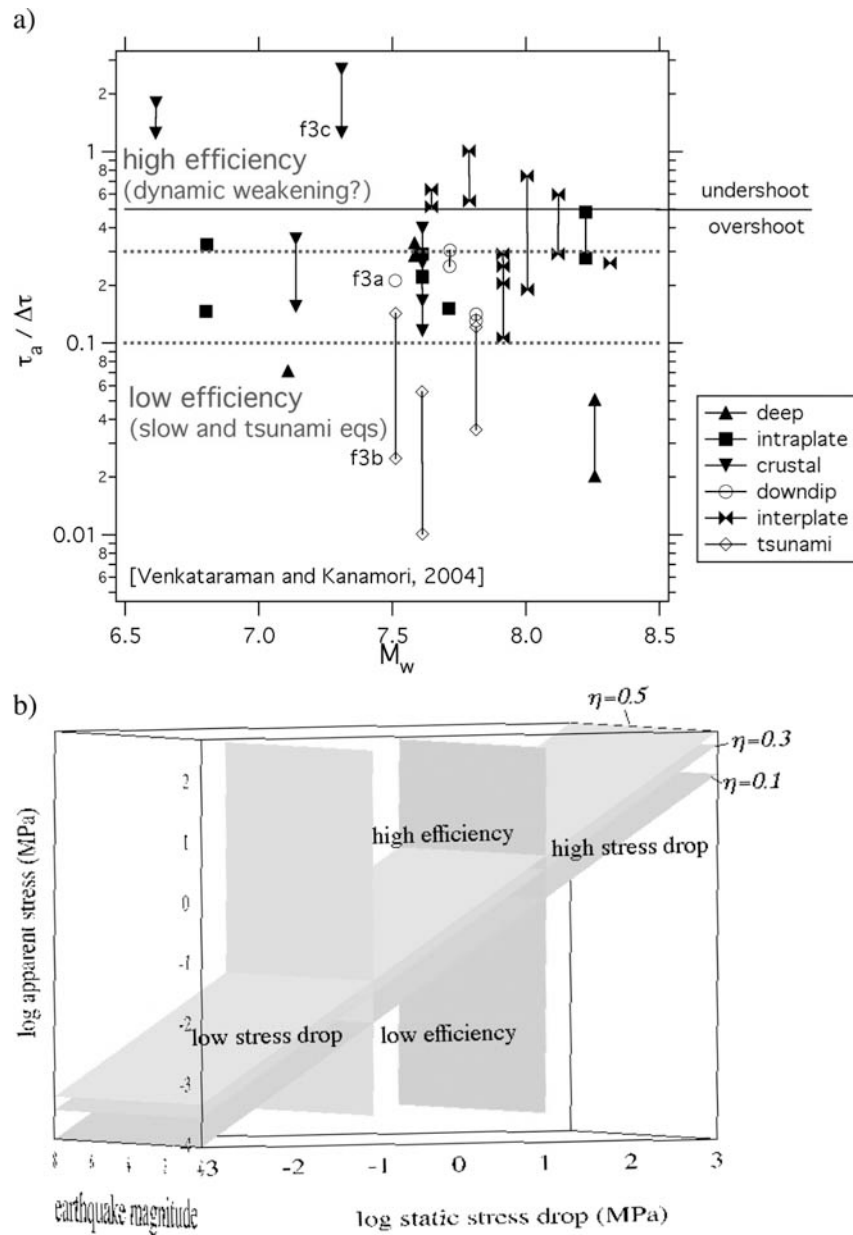


**Figure 4.** Classifying earthquake source properties. a) The efficiency of large earthquakes, from various tectonic settings [Venkataraman and Kanamori, 2004]. Horizontal lines define high, low and typical efficiency inferred from lab and mining-induced earthquakes [McGarr 1994, 1999]. Efficiency of 0.5 is the boundary between overshoot and undershoot. Lines connecting points indicate the range in estimates of efficiency. b) 3D classification plot for earthquakes. Axes are apparent stress (y), static stress drop (x) and seismic moment (z). The two vertical planes are Hanks' [1977] bounds on typical stress drop. Sloped planes (0.1, 0.3, 0.5) are constant efficiency. Typical earthquake source properties lie within the included region.

correspond to typical, high and low efficiency earthquakes are shown in Figure 3. These are energetically identical to specific earthquakes of Figure 4. On the basis of the efficiency of low temperature, low normal stress, short slip lab experiments and small mining-induced events discussed by McGarr [1994; 1999] (see section 5), Beeler *et al.* [2003] suggested efficiency greater than 0.3 is evidence of dynamic weakening in excess of typical. Efficiency of 0.5 is the boundary between overshoot and undershoot. If these data are representative of large earthquakes, undershoot would be only somewhat unusual. At the low end, efficiencies less than 0.1 are anomalous but also not uncommon. Such inefficient events correspond to slow and tsunami earthquakes [Venkataraman and Kanamori, 2004]. Though (7) gives no particular insight, Venkataraman and Kanamori's interpretation of these as high fracture energy earthquakes is a likely explanation.

So, source energy partitioning is variable, perhaps representing multiple physical mechanisms at the source. To better distinguish between different types of earthquakes using observational seismology, it may be useful to consider deviations from the typical, of both static stress drop and efficiency and as a function of earthquake magnitude, as in Figure 4b. Bounds on typical static stress drop (0.1 to 10 MPa, vertical planes) are given by Hanks [1977]. Sloped planes are constant efficiency, 0.1, 0.3 and 0.5 are shown. Typical earthquakes plot in the included area between the sloped and vertical planes. Above the top planes is high efficiency, below the lower plane is low efficiency. Venkataraman and Kanamori's compilation of large events is the only study to classify earthquake source properties in this manner. Laboratory studies of shear-induced weakening processes can contribute to understanding source physics by identifying the high slip rate fault properties manifest as stress drop and efficiency in seismic data.

### 3. ROLE OF LABORATORY OBSERVATIONS IN THE STUDY OF EARTHQUAKE SOURCE PROPERTIES

The objectives of a lab study are to access a process and characterize it sufficiently for modeling and analysis of natural observations. In nature, the conditions permitting a particular processes can be limited in strain, strain rate, temperature, fluid pressure, and time. Establishing the range of conditions over which a process occurs outside the lab can only be done by comparing with known competing processes. Given the number of potential processes and the complex geometry and heterogeneity associated with large earthquake rupture, extrapolating laboratory observations requires numerical and theoretical modeling beyond the expertise of most lab researchers.

#### 3.1 Lab Measurements Necessary for Constitutive Relations of Dynamic Fault Strength

It is usually not possible to reproduce all natural conditions in a single experiment, particularly average slip rate and total slip. So, a successful study will determine the material constants and other variables and establish the range of conditions over which the process occurs.

For comparison with seismological source parameters, unfortunately, most lab testing procedures do not measure apparent stress, efficiency or static stress drop directly. Usually a quasi-static strength reduction is measured instead. This strength loss is the lab equivalent of earthquake dynamic stress drop. The static stress drop could be inferred indirectly from lab data if overshoot were known, or from simulations using constitutive relationships based on the lab measurements.

With reference to Figure 5, to construct useful constitutive relationships for fault strength during rapid slip there are 4 essential properties to characterize:

**3.1.1 Yield strength.** Determining the yield strength and its dependencies stipulates the stress state during slip onset and fixes the initial heat production rate. As you'll see throughout the remainder of this paper, the yield strength is generally determined by conventional low temperature rock friction, has a strong normal stress dependence and is largely independent of strain rate and temperature.

**3.1.2 Strength loss.** For relating lab observations to the earthquake source use the maximum strength loss, equivalent to the source 'dynamic stress drop'  $\Delta\tau_d$ , the difference between the yield strength and the minimum strength (Figure 5). More generally, and especially in cases where

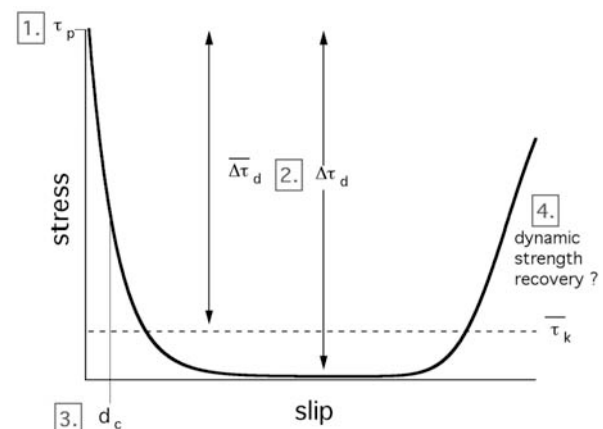


**Figure 5.** General characteristics of fault strength to be determined in lab tests. See text for discussion.

there is significant slip weakening or strength recovery it's useful also to consider the slip averaged strength loss  $\Delta\bar{\tau}_d = \tau_p - \bar{\tau}_k$  (Figure 5).

With the exception of dynamic rupture propagation in large samples (see section 5), the initial stress and yield stress in lab tests are equivalent and the pre-stress is zero. Because of the expected differences between natural and lab pre-stress, if overshoot is positive then lab-measured strength loss is the minimum static stress drop. For undershoot, lab-measured strength loss represents the maximum possible static stress drop. When pre-stress is zero, static stress drops might be further constrained by

$$\Delta\tau = \frac{\Delta\bar{\tau}_d}{(1-\xi)}, \quad (8)$$

if overshoot can be somehow inferred from lab tests. Care in estimating the appropriate slip to use in averaging the strength loss is required because total slip in lab tests is usually much smaller than natural coseismic slip.

For extrapolation to natural conditions the dependencies of strength loss on normal stress and slip rate are needed. The physical mechanism controlling the dynamic strength is a key for extrapolating lab data.

**3.1.3 Characteristic weakening distance.** The weakening distance  $d_c$  associated with the strength loss determines the fracture energy (2). In dynamic rupture models fracture energy influences the slip speed, rupture propagation rate and radiated energy. Estimates of fracture energy can be made by assuming an exponential strength loss with slip  $\delta$ ,  $\Delta\tau_d \exp(-\delta/d_c)$  so that (2) is

$$G_e = \Delta\tau_d d_c. \quad (9)$$

Extrapolating (9) depends on whether  $d_c$  is determined by fault surface asperity size or other factors. In all known cases, the effective shear fracture energy in faulting experiments is heat, rather than surface energy.

**3.1.4 Dynamic strength recovery.** The mode of rupture propagation, enlarging crack or slip pulse, depends on the stress state and whether that the fault strength can increase due to local conditions (slip rate, time, slip). When pre-stress is zero, if the fault weakens and cannot recover, rupture propagates as an enlarging crack, leading to typical or low efficiency and overshoot. Conversely, self-healing slip pulses are associated with high efficiency and undershoot. Knowing whether overshoot is positive or negative aids in estimating static stress drop (8). Mechanisms with negative rate dependence, such flash melting (section 6.2) allow self-healing and the stronger the rate dependence the greater the tendency to

self-heal. *Zheng and Rice* [1998] provide analytical expressions with which to analyze self-healing.

#### 4. CONVENTIONAL FRICTIONAL AND LOW TEMPERATURE ROCK DEFORMATION

When slip rates are below a few tenths of m/s, and total slip is limited to a few 100  $\mu\text{m}$  significant strength losses are controlled by the same mechanisms that determine static and low slip rate fault strength, conventional rock friction [Byerlee, 1978], with nearly linear pressure dependence and weak dependence on slip rate [Dieterich, 1978; 1979]. For sliding on bare rock surfaces, normal force  $F_n$  is concentrated at a few asperity contacts on the surfaces. The average asperity normal stress is determined by the material yield strength usually equated with the indentation hardness [e.g., Dieterich and Kilgore, 1996],  $\sigma_c = F_n/n\bar{A}_c$  where  $n$  is the number of contacts and  $\bar{A}_c$  is average asperity contact area. The macroscopic effective normal stress is  $\sigma_e = F_n/A$ . Shear load  $F_s$  applied to the surface causes shear displacement, limited by the average contact shear strength, again a material constant,  $\tau_c = F_s/n\bar{A}_c$ . The macroscopic shear stress is  $\tau = F_s/A$ . Thus the macroscopic shear  $\tau = \tau_c \bar{A}_c/A$  and effective normal stress  $\sigma_e = \sigma_c \bar{A}_c/A$  can be written without specific reference to the forces and the result qualitatively explains the observation that the macroscopic ratio of shear stress to effective normal stress

$$f = \frac{\tau}{\sigma_e} = \frac{\tau_c}{\sigma_c} \quad (10)$$

is approximately independent of normal stress.

##### 4.1. Yield Strength

Estimate yield strength (Figure 6),  $\tau_y = f \sigma_e$ , from the effective normal stress and laboratory measures of  $f$  [e.g., Byerlee, 1978; Paterson and Wong, 2005].

##### 4.2 Strength Loss

For smooth laboratory faults strength losses increase nearly linearly with normal stress in unconfined tests with the constant of proportionality of 0.11 to 0.08 MPa/MPa for quartzofeldspathic and other strong silicate rocks [Johnson et al., 1973; Okubo and Dieterich, 1984; Wong, 1986] (Figure 6). The strength loss results from a weak logarithmic dependence of friction on sliding velocity  $V$ , represented in detail using rate and state variable relationships [Ruina, 1983]. The net rate dependence of friction is -0.001 to -0.004 =  $df/d \ln V$  and is thought to result from reduction of contacting area with slip rate, implying shear-induced dilatancy [e.g., Scholz and Engelder, 1976].

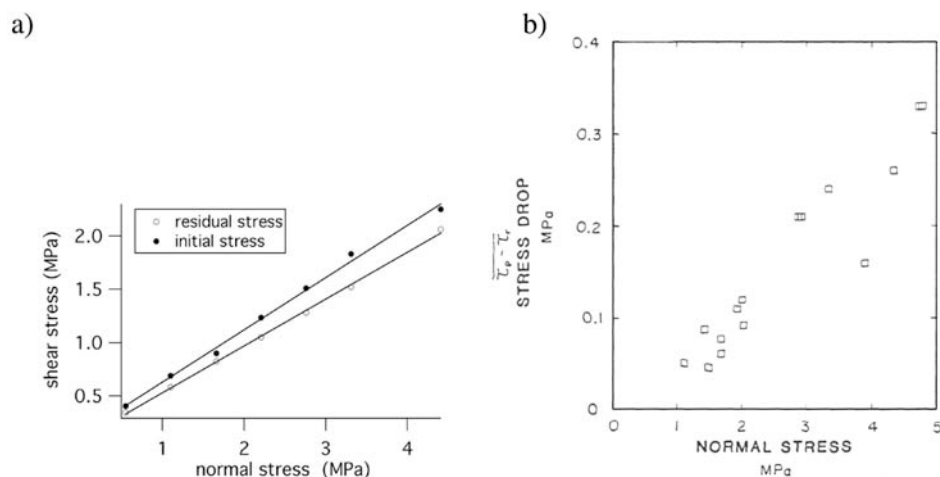


**Figure 6.** Yield strength and strength losses accompanying rapid slip in conventional low temperature friction experiments a) Initial and residual stress. [Lockner and Okubo, 1983]. b) The strength loss, defined by the difference between initial and residual stresses [Okubo and Dieterich, 1981].

#### 4.3 Slip Weakening Distance and Fracture Energy

The slip weakening distance increases with increasing surface roughness, is independent of normal stress (Figure 7) and proportional to average contact asperity size [Okubo and Dieterich, 1984]. The effective fracture energy is approximately linear in normal stress (Figure 7). Due to low surface roughness and normal stress there is little microcracking and comminution associated with shear, meaning that most of the energy dissipated by faulting is heat rather than fracture surface energy. Attempts to measure shear heat associated with rapid slip are consistent with this interpretation [Lockner and Okubo, 1983]. Fracture energy from these lab tests and those of Okubo and Dieterich [1981; 1984] can be extrapolated to larger events by assuming a particular rupture model, e.g., McGarr *et al.*, [2004] who used Madariaga [1976]. In Madariaga's model, as in all dynamic rupture models, the fracture energy limits the rupture propagation speed, so lab observed rupture speeds, slip and stress drops scaled to natural conditions can be used to estimate a scale-dependent effective fracture energy. These are consistent with typical natural earthquakes, meaning that these lab events have fracture energies that are a similar proportion of the available energy as for typical earthquakes.

A different extrapolation of effective shear fracture energy and characteristic length considers the roughness of natural faults, joints [Brown and Scholz, 1985; Power *et al.*, 1987], and the surface traces [Scholz and Aviles, 1986]. For natural fault traces and exposed fault surfaces, measures of surface roughness increase with distance along the fault surface trace [Scholz and Aviles, 1986; Power *et al.*, 1987] requiring small

ruptures to have lower surface roughness than large ruptures. Slip along rough surfaces leads to wear, the breaking and subsequent comminution of the surface roughness, and wear increases with surface roughness [Power *et al.* 1988; Scholz, 1987]. Therefore the amount of dissipation due to wear is expected to increase with rupture size (roughness) and with slip.

*4.3.1 Generalities about fault strength and energy dissipation in low temperature rock deformation.* All of the above inferences about source parameters also apply to low temperature intact rock failure. Intact rock failure tests can be associated with rapid unstable slip [e.g. Brace and Byerlee, 1966] or can be controlled in a stiff testing machine [Wong, 1982; Lockner and Byerlee, 1992]. In controlled experiments (Figure 8) failure strength, residual strength, and fracture energy are measured directly. Yield strength and strength loss increase with normal stress (Figure 8d). The slip weakening distance is independent of normal stress and effective shear fracture energy increases linearly with normal stress (Figure 8e).

Unlike slip on pre-existing faults, intact failure involves the creation of a complex fault surface and attendant off-fault damage. By carefully accounting for the number and size of stress-induced microcracks during rock failure, Wong [1982] found that the energy inferred from integrating to obtain the shaded area in Figure 8c  $\sim \Delta\tau_d \delta_w A / 2$ , is 10 to 100 times greater than the energy stored in new fracture surface area  $2\Gamma S_v w$ , where  $S_v$  is the surface area per unit volume that is created as the crack advances, and  $w$  is the fault zone width. In contrast, for tensile rock stress/strain determined fracture

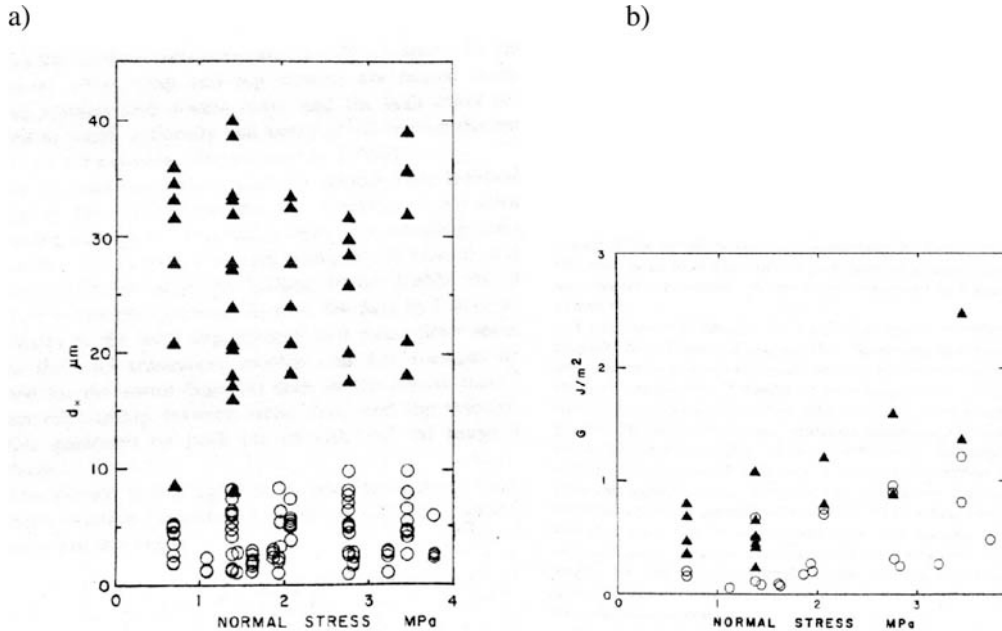


**Figure 7.** Weakening distance and fracture energy for conventional low temperature friction. [Okubo and Dieterich, 1984]. Two different roughness faults are shown (rough triangles, smooth circles) a) Distance to slip weaken. b) Fracture energy.

energy and associated micro-crack surface energy are equal [Friedman *et al.*, 1972]. This suggests that effective shear fracture energy is heat and that the energy expended during the breakdown of fault strength is much larger than the true shear fracture energy.

#### 4.3.2 Surface energy associated with wear and damage.

However, these analyzes do not include fracture surface energy associated with gouge formation and comminution. Sliding on nominally flat but roughened surfaces at normal stresses as low as 25 MPa produce highly comminuted wear products with grain diameters approaching unit cell dimension ( $< 10$  nm) [Yund *et al.*, 1990]. Assuming spherical particles and constant porosity, surface area varies inversely with grain size, so very highly comminuted wear product could have large associated surface energy. Estimates based on Yund *et al.* [1990] do not show large surface energy relative to the total dissipated energy, however those experiments were at slow and stable sliding rates. Given that one recent estimate of surface energy of rock flour generated by seismic faulting in deep gold mines is similar to frictionally generated heat [Wilson *et al.*, 2005] new measurements of surface energy in lab stick slip and intact failure tests are warranted.

Lab measured surface energy and other forms of damage associated with rapid slip are incomplete because there is no

dynamic stress field associated with the tip of the propagating rupture. The large local dynamic stress change due to slip on naturally rough fault surfaces does not arise in lab samples. Even in large experiments where the slip does propagate, the slips are small and faults are essentially flat so off-fault damage is negligible. Without future innovations the complete contributions of damage including a comprehensive accounting of true surface energy during dynamic rupture is outside the scope of laboratory investigations. It is well-known from theoretical analysis that high off-crack stresses induce branching, or additional inelastic processes which increase the shear fracture energy associated with propagation [e.g., Andrews, 1976; Rice, 1980]. Thus, any realistic earthquake rupture model will require stress to be limited by the yield criterion, and the effective shear fracture energy must increase with the propagation distance [Andrews, 1976]. Andrews [1976; 2005] has considered this issue most rigorously by representing the off-crack behavior in elastodynamic rupture propagation calculations as elastic-plastic instead of purely elastic and finds propagating rupture has effective shear fracture energy that increases linearly with crack length. Similar arguments for static shear fracture have been made by Cowie and Scholz [1992] based on Dugdale's [1960] elastic-plastic cohesive zone model for tensile fracture. Further lab contributions might involve a complete accounting of damage (crack surface area,

surface area of comminuted material, and heat) than have been used in the simple theoretical models to date.

4.4 Strength Recovery and Overshoot

On the timescale of a dynamic event, strength loss in friction and in rock fracture tests is effectively permanent, that is, strength recovery occurs over a longer timescale than the event

itself. This is because the steady-state rate dependence of low temperature rock friction is small, so as slip begins to decelerate the strength goes up only slightly. And it only increases briefly; as soon as the slip velocity has decreased slightly fault strength deviates from steady-state and while slip decelerates fault strength is effectively rate strengthening. At this stage fault properties cannot induce local strength recovery, arrest must result from propagating elastodynamic stopping phases,

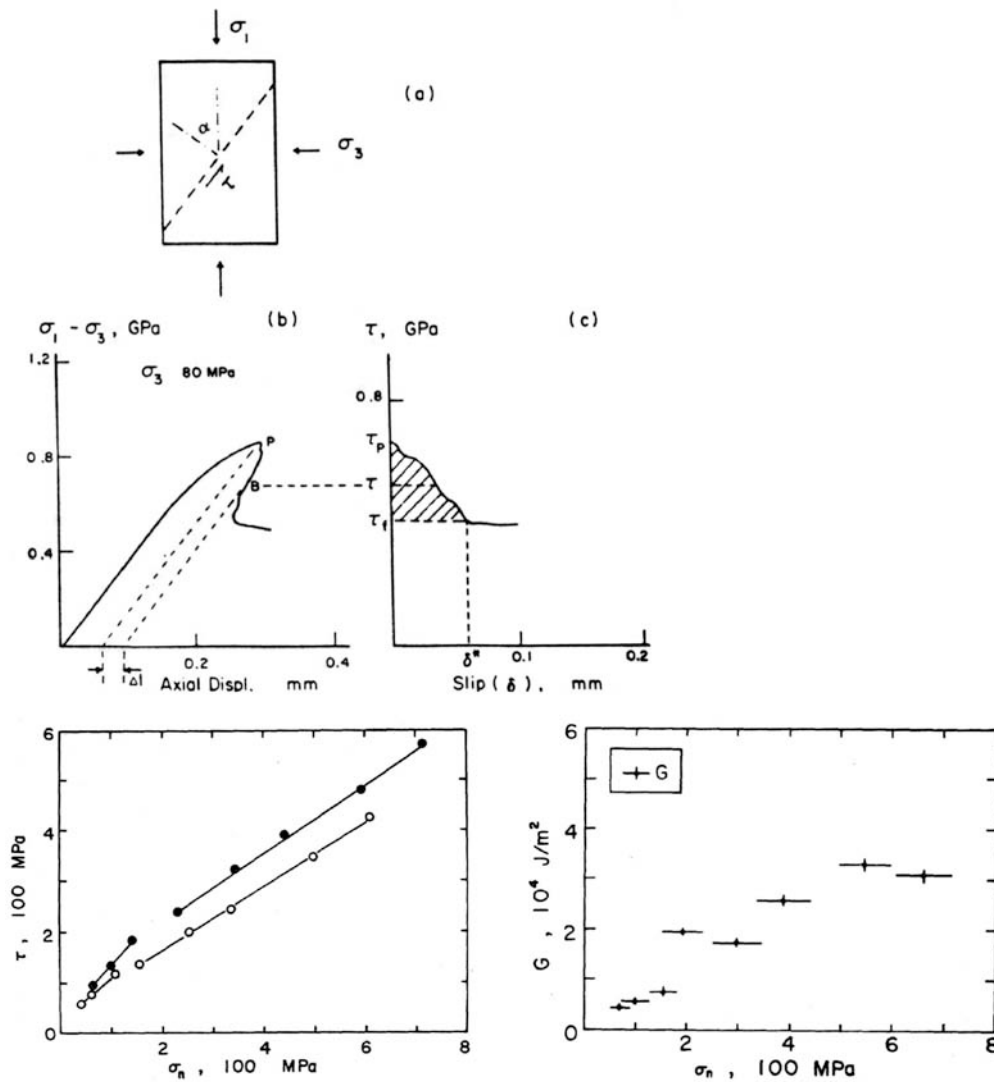


**Figure 8.** Summary of strength data from intact rock failure tests of Wong [1986]. a) Failure test geometry, a cylindrical sample and 2 independently controlled applied stresses, axial and confining stresses. b) Differential stress vs. axial displacement. c) The shear stress and fault displacements corresponding to b). d) Shear and normal stress associated with peak (solid) and residual strengths (open) collected from a sequence of tests at different normal stresses. e) Effective shear fracture energies calculated from a sequence of failure tests, each having data like shown in c), using equation (2).

and stress will overshoot the slip averaged shear resistance leading to typical or low efficiency.

### 5. IMPLICATIONS OF STICK-SLIP EXPERIMENTS FOR THE SOURCE TIME FUNCTION

Laboratory approaches to studying the earthquake source divide naturally into two types. There are ‘stick-slip’ experiments [Brace and Byerlee, 1966] where elastic strain stored in the sample and testing machine during loading is released in a rapid slip event - the loading being conducted at a rate slower and nearly unrelated to the speed attained in the rapid event; these are the lab analogue of an earthquake. Most have been conducted at slips and slip speeds within the range of conventional friction and for that reason are discussed in this section. In the other type of rapid slip experiments the fault is actively driven at a prescribed high slip rate. Results from those experiments will be discussed in the subsequent section 6.

Source time functions from analogue laboratory earthquakes (Figure 9a) are similar to the ramp functions of simple source models (Figure 9b) [e.g., Brune, 1970], but there are important differences in interpretation [Shimamoto *et al.*, 1980]. Due to low normal stress and the characteristics of laboratory testing equipment, slip speeds in stick-slip experiments can be lower than would be inferred from a plane wave resulting from a natural dynamic stress drop ( $V = 2\Delta\tau_d \beta/\mu$ , e.g. Brune [1970]), and the duration of slip can be controlled by machine characteristics rather than those of the fault itself. Because sample sizes are small and rock modulus is large, most laboratory faults are effectively rigid, that is, there is no dynamic rupture propagation. An appropriate model for this kind of stick-slip stress drop is a slider block [Johnson *et al.*, 1973; Shimamoto *et al.*, 1980; Rice and Tse, 1986]. Using this model, the event duration is at least half the characteristic period  $T$  of the testing machine ( $T/2 = \pi\sqrt{m/k}$ ,  $m$  is mass per unit fault area and  $k$  is stiffness). Total slip is  $s = \Delta\tau/k$ , so the average slip speed is related to stress drop as

$$V \approx \frac{\Delta\tau}{\pi\sqrt{mk}}, \quad (11)$$

rather than through the shear impedance as in simple elastodynamic estimates [Johnson and Scholz, 1976; Shimamoto *et al.*, 1980].

In typical tests at 5 to 25 MPa normal stress, per event slip is low, e.g.,  $s = 100 \mu\text{m}$  and the machine time constant is on the order of a millisecond [Shimamoto *et al.*, 1980]. Thus, typical stick-slip slip speeds are in the range of 0.1 m/s. Much higher slip speeds could be attained by using test equipment with lower effective mass or lower stiffness; the recent study by Koizumi *et al.* [2004] which reports average slip speeds of 15 m/s may be an example of this approach. Another way to

attain higher slip speed is to conduct experiments at higher normal stress, since the strength losses for conventional friction increase linearly with normal stress. Alternatively, much higher stress drops can be achieved artificially using a torsional Kolsky bar [Prakash, unpublished]. In such an apparatus a cylindrical sample is attached to the end of a long, precision ground high strength metal bar; the sample is placed in contact with a fixed flat surface and loaded normal to its axis. The bar is held fixed at the sample end and torqued at the opposite end, then the sample end is unclamped transmitting a shear stress change exceeding what the loaded sample surface can naturally sustain [Prakash, unpublished]. High speed stick-slip experiments either at high normal stress or with a specialized testing apparatus are largely unexplored at present.

Another serious limitation of laboratory stick-slip as a valid analogue for natural earthquake source properties result from differences in the equations of motion. As a result of these differences, when slip is unconfined, slip overshoots, requiring that energy partitioning be constrained to low and typical efficiencies. This can be understood by using the equation of motion for a slider block, accounting for radiation,

$$k \left( \frac{T}{2\pi} \right)^2 \frac{\partial^2 \delta}{\partial t^2} = \tau - \tau - \frac{\mu}{2\beta} \frac{\partial \delta}{\partial t} \quad (12)$$

[Rice, 1993], where  $\tau$  is stress,  $\tau$  is strength,  $\delta$  is slip and the last term on the right hand side is the radiated energy term (radiation damping). Slip accelerates when the sum of the fault strength and radiation damping term is less than the stress,

$$\tau > \tau + \frac{\mu}{2\beta} \frac{\partial \delta}{\partial t},$$

and maximum slip speed corresponds to zero acceleration at

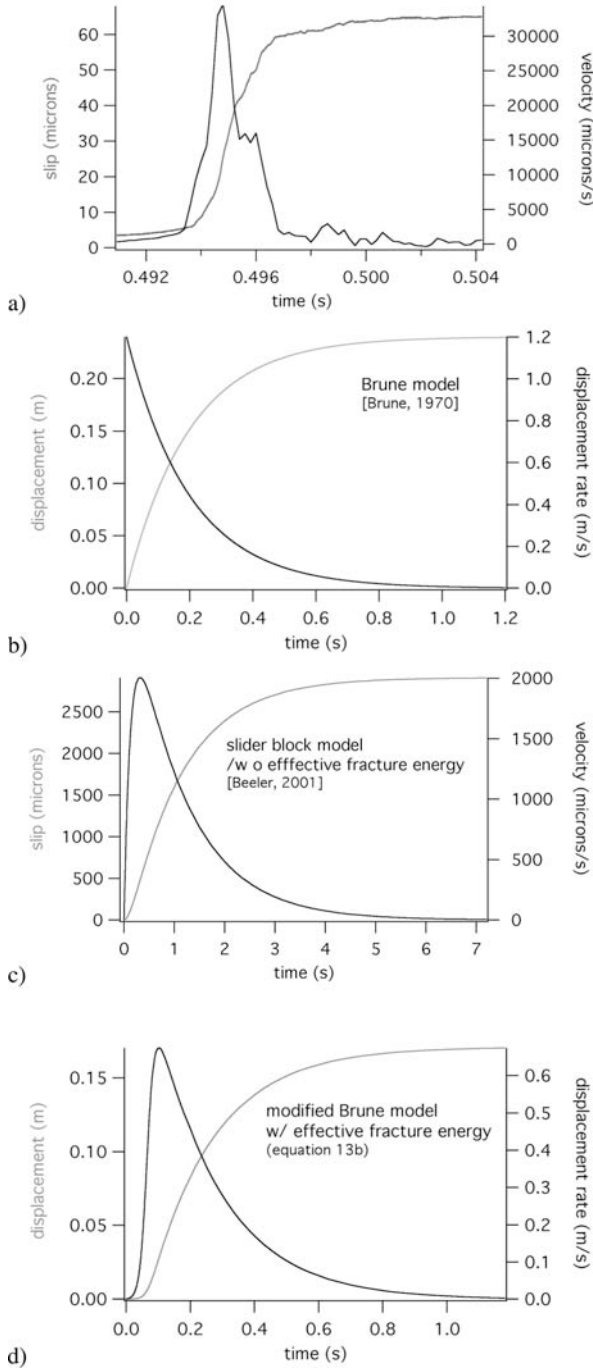
$$\tau = \tau + \frac{\mu}{2\beta} \frac{\partial \delta}{\partial t}.$$

Deceleration occurs when the available stress is

$$\tau < \tau + \frac{\mu}{2\beta} \frac{\partial \delta}{\partial t}.$$

At full arrest  $d\delta/dt$  is zero such that the final condition is  $\tau < \tau$  and stress always overshoots the fault strength. In practice, a slider block is only a crude model of a stick-slip experiment but it is impossible to interpret arrest in stick-slip experiments as being due solely to changes in fault strength. For example, Koizumi *et al.* [2004] interpret arrest as resulting from melting in a stick-slip experiment at a stage where deceleration and arrest due to inertial forces are inevitable.

Similarly, because of inertia, slip onset in a stick slip lab experiment is gradual, and would be so even if strength loss were instantaneous (Figure 9c), as illustrated in the



slider block solution given by *Beeler* [2001]. So, care in interpretation of lab source slip-time characteristics is necessary.

*Dynamic rupture propagation experiments.* On the otherhand, evidence of gradual slip onset in true rupture propagation experiments is pervasive [e.g., *Okubo and Dieterich*, 1984; *Ohnaka et al.*, 1986] and indicates an effective shear fracture energy (Figure 1), neglected in some seismic source models, for example the Brune model

$$\dot{u} = \frac{\Delta\tau_d\beta}{\mu} \exp\left(-\frac{t}{t_c}\right), \quad (13a)$$

(13a) could be modified to include displacement weakening, e.g.,

$$\dot{u} = \frac{\Delta\tau_d\beta}{\mu} \left(1 - \exp\left(-\frac{u}{u_c}\right)\right) \exp\left(-\frac{t}{t_c}\right) \quad (13b)$$

where  $u = \delta/2$  is displacement, and  $u_c = d_c/2$ . The source time function of (13b) is

$$t = -t_c \ln \left\{ -\frac{1}{t_c} \left[ \frac{\mu}{\Delta\tau_d\beta} \left[ u + u_c \ln \left( 1 - \exp\left(-\frac{u}{u_c}\right) \right) \right] \right] \right\} \quad (13c)$$

(Figure 9d).

Most dynamic rupture experiments [*Johnson and Scholz*, 1976; *Okubo and Dieterich*, 1984; *Ohnaka et al.*, 1986] propagate to the ends of the fault prior to arrest. At that stage a mixed behavior results and slip arrest becomes influenced by the machine. Slip duration is at least as long as the machine time constant, just as for stick-slip tests. In contrast, confined experiments such as *Lockner et al.* [1982] have duration determined by the rupture propagation speed and fault dimension as expected from crack models of natural expanding ruptures. The confined events overshoot and do not show large differences in source partitioning. The conclusion from limited studies (Figure 10) is that the efficiencies are typically 0.1 to 0.3, similar to mining-induced

**Figure 9.** Comparison between lab and seismic source time functions. Slip (or displacement) (left axis) and velocity (or displacement rate) (right axis). a) Unconfined dynamic rupture propagation test in Dieterich's 2 meter fault press. [*Kilgore*, unpublished] with gradual onset due to effective shear fracture energy. Event duration is determined by machine characteristics. b) Brune source with no fracture energy or inertia, and characteristic slip duration  $t_c$  controlled by rupture dimension and propagation speed [*Brune*, 1970]. c) Slider block model with radiation, has inertia but no fracture energy. Gradual onset is due to inertia. Duration is determined by machine characteristics [*Shimamoto et al.*, 1980]. d) Modified Brune model with an effective shear fracture energy (13).

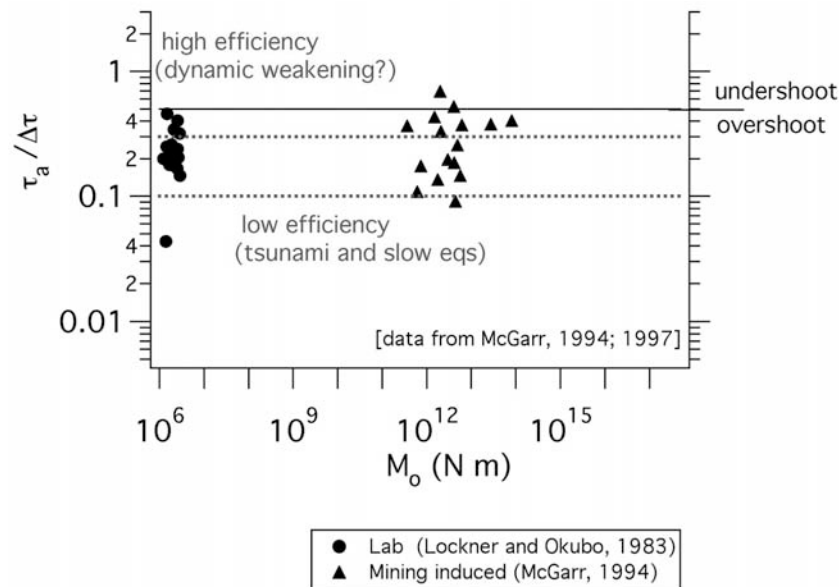


**Figure 10.** Small earthquake efficiency, for comparison with large earthquakes (Figure 4). Data are from mining induced earthquakes [McGarr, 1994] (solid triangles) and from laboratory stress drops (solid circles) [Lockner and Okubo, 1983]. The horizontal lines define high, low and typical efficiency. 0.5 is the boundary between overshoot and undershoot.

events and estimated efficiencies from larger earthquakes [McGarr, 1994; 1999]. Extrapolation of the maximum slip, average slip and maximum apparent stress of these lab events to large earthquakes shows very good agreement [McGarr and Fletcher, 2003], confirming that energy partitioning resembles typical earthquakes.

#### 6. HIGH STRESS DROP AND HIGH EFFICIENCY MECHANISMS

A comparison between efficiency of lab events and large earthquakes (Figures 4 and 10) shows that higher and lower efficiencies do occur in nature. While higher efficiencies cannot be addressed directly in lab tests there is some evidence from stick-slip experiments of higher stress drops than an extrapolation of Lockner and Okubo [1983] (Figure 11). At higher normal stress, stress drops are larger consistent with a change in mechanism controlling dynamic fault strength. While observations such as shown in Figure 11 are not uncommon [e.g., Summers and Byerlee, 1977; Gu and Wong, 1994] the triaxial geometry used is not ideal; there is dynamic unloading of normal stress and a kinematic requirement of slip at one of the two piston-rock interfaces that are normal to  $\sigma_1$ . More reliable data can be collected using high speed rotary shear where the sliding speed is a control variable rather than a result of fault and machine properties [Tsutsumi and Shimamoto, 1997; Goldsby and Tullis, 2002]. In controlled tests weakening mechanisms thought to result from

phase changes on the fault surface have been activated as slip speeds exceed 1 mm/s, even when shear heating of the fault is well below melting.

#### 6.1 Unexpected Weakening at Sub-Seismic Slip Rates

Tests conducted on initially bare surfaces of silica-rich rocks (quartzite, novaculite, feldspar, and granite) to slips greater than a few meters at slip speeds from 10 mm to 0.1 m/s show a large strength loss (Figure 12a) [Goldsby and Tullis, 2002; DiToro et al., 2004], whereas less silica-rich (gabbro) and silica-absent rocks (marble) show no weakening. Measurements and calculations indicate asperity contact temperatures less than 140 °C, and average temperatures 10's of degrees less. It has been proposed based on inference and microstructures that shear lubricates the surface through production of a highly comminuted and amorphous material which may be silica gel. Temperature is not involved as changes in strength occur more slowly than temperature change when the velocity is increased or decreased. As noted first by David Lockner, the primary observations are well explained a 'thixotropic' fault, a near-fluid that becomes more less viscous (weaker) when strained. In the case of a gel, the weakening results from dynamic reduction of the number of chemical bonds. When shearing ceases the material regains strength with time at a rate controlled by the bond forming chemical reaction.

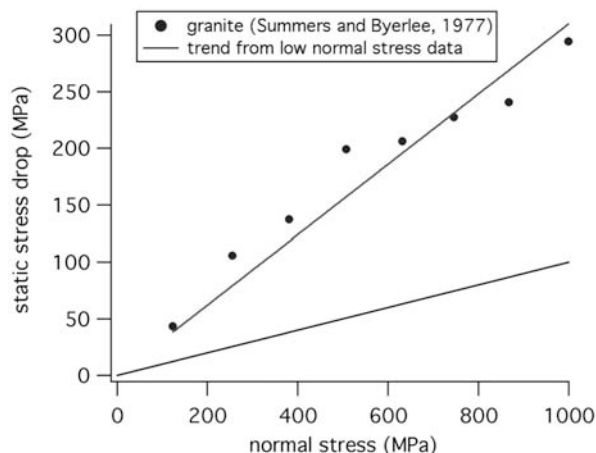


**Figure 11.** Lab data showing higher stress drop at higher confining pressure. Stick-slip data from Westerly granite at high normal stress from *Summers and Byerlee* [1977] (blue dots). The linear fit to this data (slope 0.31) is constrained to have zero intercept. For reference is the extrapolation of the low temperature friction data on Sierra granite from *Okubo and Dieterich* [1984] with slope of 0.1.

**6.1.1 Yield strength.** The yield strength is due to conventional rock friction.

**6.1.2 Strength loss.** Strength losses are large, slip rate (Figure 12b) and normal stress (Figure 12a) dependent [*Goldsby and Tullis*, 2002; *DiToro et al.*, 2004]. The residual strength itself is normal stress dependent, e.g., if expressed as friction at 0.1 m/s, strength is about 0.2. In addition, the pressure dependence is non-linear and residual friction decreases slightly with normal stress. At higher normal stress there may be more wear and a thicker gel layer having a lower shear resistance.

**6.1.3 Characteristic weakening distance and shear fracture energy.** The distance to weaken is around 1 meter and is largely independent of normal stress and time as evidenced by no systematic change in the weakening distance with strain rate (Figure 12). Some unpublished data suggest a weak increase of the weakening distance with slip rate (*T. Tullis*, pers. comm.). The weakening distance may be that necessary to reach a steady state thickness of a wear generated lubricant and may scale with surface roughness. Since the strength loss and weakening distance are large, this mechanism will produce very large effective shear fracture energy in comparison to conventional rock friction. Fracture energy will increase nearly linearly with normal stress.

**6.1.4 Dynamic strength recovery.** Recovery to the yield strength occurs quickly and experiments demonstrating this

unique aspect were conducted by *Goldsby and Tullis* [2002] (Figure 12c). However, the recovery occurs more slowly than the temperature change and with duration (100's of seconds) that is long with respect to earthquake rise times. Thus, it is unlikely that this mechanism would lead to self-healing and undershoot. Given the tendency towards high effective fracture energy, this mechanism could produce high static stress drop with very low efficiency for smaller earthquakes, lower and more typical efficiencies for large events.

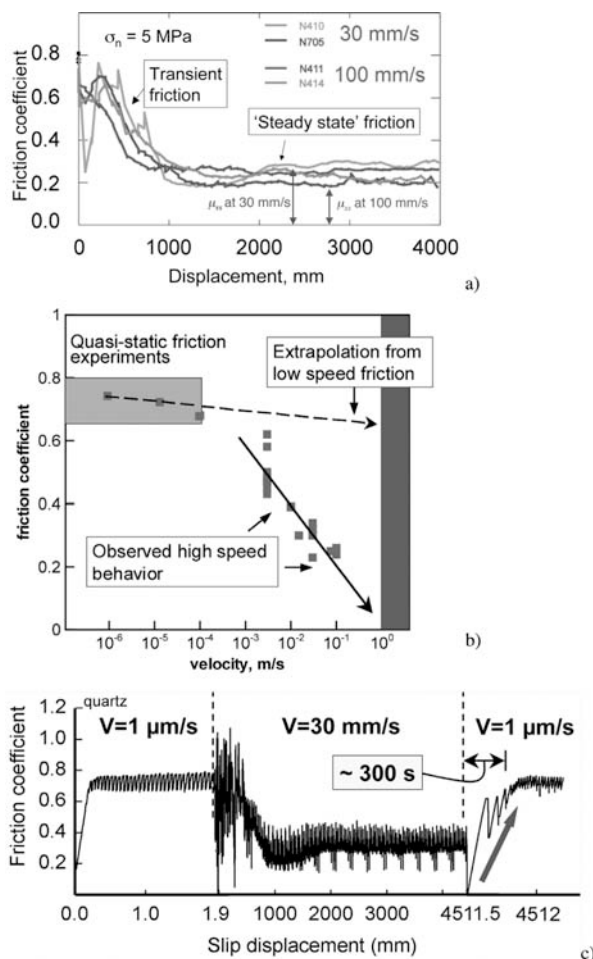


**Figure 12.** Unexpected and extraordinary slip weakening. a) Novaculite at 5 MPa normal stress at two different sliding rates [*DiToro et al.*, 2004]. b) The dependence of friction on slip rate. Low temperature friction data are shown for comparison. The solid line is one possible extrapolation to higher slip rates. c) Summary of strength loss and strength recovery due to unexpected weakening. Friction coefficient with slip at 1  $\mu\text{m/s}$ , 30 mm/s, and again at 1  $\mu\text{m/s}$ . Note the scale of the horizontal axis changes with velocity [*DiToro et al.*, 2004].

### 6.2 Flash Weakening

Experiments on initially bare surfaces at slips to a few tens of mm and up a few tenths of m/s show dramatic weakening [Tsutsumi and Shimamoto, 1997; Goldsby and Tullis, unpublished; Prakash, unpublished] (Figure 13). Total slip is too small for these results to be explained by the unexpected weakening of section 6.1 and the durations (0.1 to 1 s) are too small to produce changes in average temperature large enough to induce bulk melting. Experiments have been conducted on gabbro [Tsutsumi and Shimamoto, 1997; Goldsby and Tullis, unpublished], quartz, granite, calcite marble [Goldsby and Tullis, unpublished], and soda lime glass [Prakash, unpublished; also see Rempel, 2006]. All of these materials weaken in approximately the same manner with the exception of marble. It is thought that weakening is due to a temperature induced phase change (melting) at highly stressed asperity contacts. The observations are consistent with a simple heat balance at asperity contacts [Rice, 1999] that predicts the onset of melting at slip speeds the range of 0.1 to 0.3 m/s, and results in a  $1/V$  dependence of fault strength on sliding velocity.

$$f = f_o, \quad V < V_0$$

$$f = (f_o - f_w) \frac{V_0}{V} + f_w, \quad V > V_0, \quad (14)$$

where  $f_o$  and  $V_0$  are friction and slip speed, respectively, at the onset of flash melting and  $f_w$  is a limiting strength due to the melt's shear resistance. (Figure 13). In addition, Rice's model suggests that upon deceleration the fault will instantaneously strengthen, again following the  $1/V$  relationship, consistent with the experimental observations (Figure 13b). Another indication that this weakening is related to flash melting is that the only tested material that does not weaken is marble which undergoes a high temperature phase change to a highly refractory product and no melt [Goldsby and Tullis, unpublished].

**6.2.1 Yield strength.** The yield strength is determined by conventional rock friction.

**6.2.2 Strength loss.** Strength losses are large. The residual strength is normal stress dependent with an inferred friction minimum of about 0.2 (Figure 13b).

**6.2.3 Characteristic weakening distance and shear fracture energy.** In Rice's theory the friction length scale is the dimension of the asperity contacts. Since the asperity contact dimensions are on the order of 10  $\mu\text{m}$  and the threshold

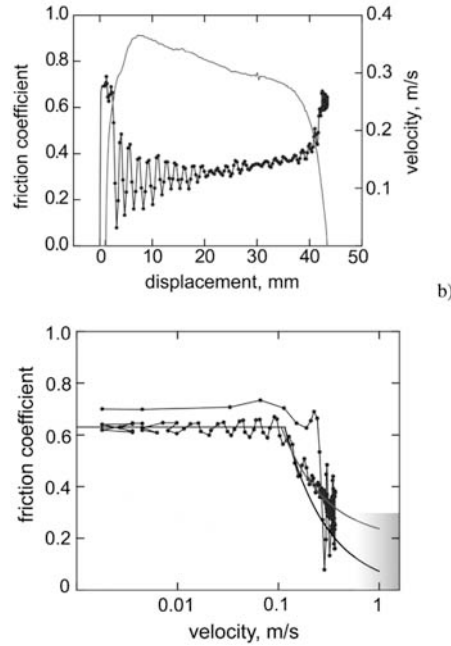


**Figure 13.** Fault strength in a laboratory test of flash weakening of quartz at 5 MPa normal stress. Test duration is about 0.2 s and the sample is slid to about 40 mm as fast as the control system will allow, reaching a peak slip velocity of around 350 mm/s. Figures courtesy of D. Goldsby and T. Tullis. a) Friction vs displacement. b) Friction vs slip velocity. Time on this plot starts at the upper left and as velocity increases out to slip speeds higher than 0.1, the strength drops rapidly. Arrest is preceded by restrengthening. Superimposed are fits to the deceleration using (14),  $f_w = 0$  (black) and  $f_w \neq 0$  (grey).

slip speed for flash is around 0.1 m/s, the time necessary to return to steady-state in response to a change in sliding velocity is  $1 \times 10^{-4}$  s and strength should be essentially always at steady-state. Therefore there is no effective slip weakening distance for lab flash processes and there is negligible associated intrinsic shear fracture energy.

**6.2.4 Dynamic strength recovery.** Fault strength tracks slip rate directly and strongly (Figure 13a). The total duration of this experiment is 0.2 s, much shorter than large earthquake rise times, so the rate of strength recovery is essentially instantaneous. This kind of direct response will tend to local arrest of rupture, undershoot and self-healing slip pulses. The existence of slip pulses for this extreme negative rate dependence was demonstrated in rupture propagation simulations by Perrin *et al.*, [1995]. Earthquakes resulting from this mechanism would have very high efficiency, and though the dynamic stress drop will be large, the static stress drops may be quite typical.

### 6.3 Bulk Melting

Rapid and large slip produces heat sufficient to cover an entire fault surface with melt [McKenzie and Brune, 1972; Sibson, 1975]. Ignoring volume loss and the latent heat of fusion, and assuming 1D heat conduction normal to the fault, the threshold duration  $t_T$  of sliding for bulk melting of the fault surface can be estimated crudely by balancing shear generated heat  $\hat{\tau}Vt_T$  against the product of the change in thermal energy, necessary to raise the temperature from  $T_f$  to the melting temperature  $T_m$ , times the width of the melted region  $\sqrt{t_T}\pi\alpha$ . Here  $\alpha$  is thermal diffusivity,  $\hat{\tau}$  is the average shear resistance, and  $\rho\hat{c}$  is the volumetric heat capacity. The threshold duration is

$$t_T = \pi\alpha \left[ \frac{\rho\hat{c}(T_m - T_f)}{\hat{\tau}V} \right]^2. \quad (15a)$$

A similar balance including the heat of fusion is considered by DiToro *et al.* [this volume] for interpreting natural shear generated melts. Assuming that the average shear resistance scales with normal stress  $\hat{\tau} = f\sigma_n$  as in conventional friction [e.g., Byerlee, 1978], given a particular slip rate, the slip necessary to produce bulk melting is

$$d_T = \frac{\pi\alpha}{V} \left[ \frac{\rho\hat{c}(T_m - T_f)}{f\sigma_n} \right]^2. \quad (15b)$$

The quantity  $\alpha_m = Vd_T = \pi\alpha \left[ \frac{\rho\hat{c}(T_m - T_f)}{f\sigma_n} \right]^2$  is the effective thermal diffusivity for bulk melting. As an example estimate of slip to melt in lab tests I use  $T_f = 25^\circ\text{C}$ ,  $f = 0.6$ , thermal constants for feldspar and low normal stresses (2 MPa) as appropriate for unconfined tests. For seismic slip rates I find that slips of the order of meters are required (Figure 14). The strong sensitivity to fault strength allows that bulk melting could be achieved in a conventional tri-

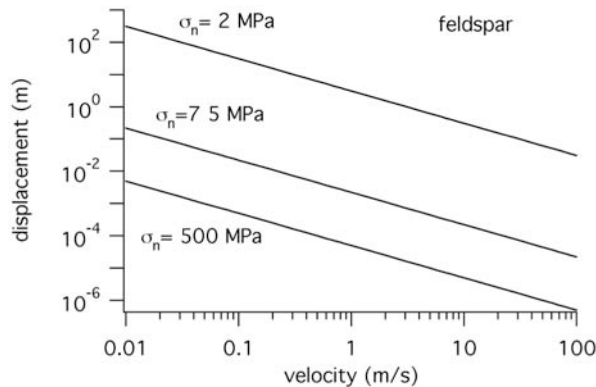


**Figure 14.** Estimate of slip needed for bulk melting of feldspar as a function of velocity for 3 choices of normal stress using equation (15b) and  $\alpha = 1.63 \times 10^6 \text{ m}^2/\text{s}$ ,  $\rho\hat{c} = 8.3 \times 10^5 \text{ J/m}^3\text{K}$ ,  $f = 0.6$ ,  $T_b = 1150^\circ\text{C}$  and  $T_f = 25^\circ\text{C}$ .

axial geometry by doing stick slip tests at high confining pressure. At 500 MPa normal stress, and a slip speed of 1 m/s, only 50  $\mu\text{m}$  slip would be necessary for bulk melting. By elevating the ambient temperature closer to the melting point, shear melting could be achieved in somewhat smaller slips, provided the rock remains brittle enough to stick-slip. Instead, the approach has been to use seismic slip speeds, low normal stress and large (often larger than seismic) slips in a rotary shear geometry. The first experiments were done by John Spray [1987; 1988] using a modified friction welding machine. Subsequent quantitative work [Tsutsumi and Shimamoto, 1997; Hirose and Shimamoto, 2005; DiToro *et al.*, this volume] has been done exclusively using rotary testing machines designed and built by Toshi Shimamoto [e.g., Shimamoto and Tsutsumi, 1994]. Experiments have been conducted on gabbro [Tsutsumi and Shimamoto, 1997; Hirose and Shimamoto, 2005], monzodiorite [Hirose and Shimamoto, 2000], granite [Lin and Shimamoto, 1998], novaculite, peridotite, tonalite, and a cataclastite [DiToro *et al.*, this volume]. These experiments indicate complications not anticipated by the balance (15).

The essential features of bulk melting tests are shown in Figure 15a, reproduced from Hirose and Shimamoto [2005]. Detailed numerical simulation of this particular laboratory test have been undertaken by Fialko and Khazan [2005] that couple shear induced heat transfer, the thermodynamics of melting, and a temperature dependent shear viscosity. With reference to that figure, following a peak strength consistent with low temperature friction there is flash weakening to low strength. So rather than as estimated in (15), the average shear resistance prior to the onset of bulk melting is much lower than Byerlee friction; still, the corresponding slip to melt are not much higher than as estimated by (15) [see DiToro *et al.*, 2005]. In addition, experiments are unconfined so wear material and melt are extruded during the experiments [Tsutsumi and Shimamoto, 1997; Hirose and Shimamoto, 2005]. As suggested by Rice [1999], at the higher normal stresses in the Earth flash melting will delay the onset of melting by lowering the shear resistance, and for small earthquakes may inhibit bulk melting altogether.

Following the strength reduction, there's strengthening due to the continued generation of melt and the additional shear resistance of viscous drag as the area of melt contact increases. Eventually the entire fault surface is covered in melt at the second peak strength [Hirose and Shimamoto, 2005]. In this example (Figure 15a), the second peak strength is higher than Byerlee friction, that is, the shear strength of the generated melt is higher than the bare fault surface. This is misleading because the first peak is strongly normal stress dependent and the second peak is very weakly normal stress dependent, if at all. Only at very low normal stress is the melt stronger than the bare rock surface [Fialko and Khazan, 2005]. Also at high normal stress, the slipped distance to get to the peak strength

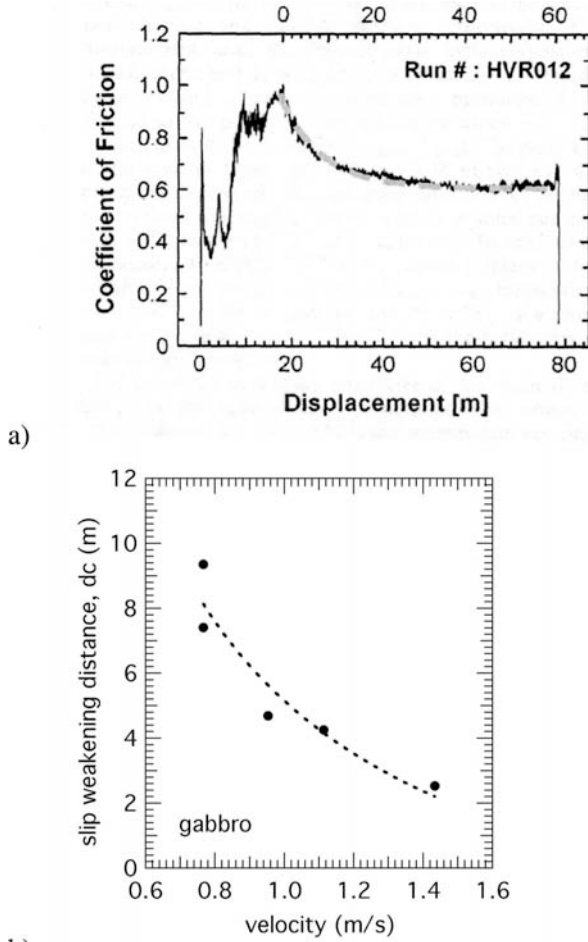


**Figure 15.** Bulk melting of gabbro. a) Friction versus displacement characteristics of bulk melting in a low normal stress laboratory test [Hirose and Shimamoto, 2005]. b) Dependence of the slip weakening distance on slip speed [Hirose and Shimamoto, 2005]. Shown is a fit to the data assuming a  $1/V$  dependence as in (16b).

is expected to be lower, according to (15). Following the second peak, resistance decreases approximately exponentially with slip as a steady-state melt thickness develops [Hirose and Shimamoto, 2005]. The slip distance decreases significantly with increasing slip velocity [Hirose and Shimamoto, 2005; DiToro *et al.*, this volume] and with increasing normal stress [DiToro *et al.*, this volume].

**6.3.1 Yield strength.** The first peak is conventional friction. The second peak is the viscous resistance of the melt, and as such should be largely independent of normal stress; this is not so in the unconfined experiments due to melt extrusion.

The pressure dependence of the second peak reflects higher extrusion rates at higher normal stress.

**6.3.1.1 Melt extrusion in experiments and nature.** Based primarily on field data of pseudotachylyte thicknesses and well-estimated ambient stresses, DiToro and co-workers have argued that similar normal stress dependence of extrusion occurs naturally. If the change in stress due to the dynamic slip associated with the propagating rupture exceeds the ambient stress, on the tensional side opening mode fractures may form at high angles to the fault surface that would dynamically drain the melt from the fault. Melting also produces a net volume increase which could lead to transient high melt pressure, hydrofracture and fluid-driven, dyke-like propagation of dynamically induced fractures. DiToro's interpretation of field data is that most of the melt generated during pseudotachylyte formation is extruded into off-fault cracks and that on-fault thickness decreases with normal stress, as in the unconfined experiments.

**6.3.2 Strength loss.** The residual strength has weak normal stress dependence [DiToro *et al.*, this volume], due to melt thickness decreasing with normal stress [Hirose and Shimamoto, 2005]; extrusion rate increases with normal stress. The residual shear resistance is due to the viscosity of the melt and at a particular rate of shearing and thickness will depend on rock type and maximum slip rate [Spray, 1993].

**6.3.3 Characteristic weakening distance and shear fracture energy.** The characteristic weakening distance depends on slip speed (Figure 18) [Hirose and Shimamoto, 2005]. This can be qualitatively understood again by using the 1D heat balance. The characteristic duration  $t_c$  of sliding to weaken the fault can be derived from balancing the shear generated heat  $\eta V^2 t_c / w$  against the product of the change in thermal energy, associated with the change in temperature  $\Delta T$ , times the width of the melted region  $w$

$$t_c = \frac{\Delta T \rho \hat{c} w^2}{\eta V^2}. \quad (16a)$$

For simplicity I've ignored extrusion, normal stress dependence and thickness changes. The associated characteristic slip is

$$d_c = \frac{\Delta T \rho \hat{c} w^2}{\eta V} \quad (16b)$$

Despite oversimplifications, the observations are consistent with a non-linear decrease in  $d_c$  with slip rate (Figure 15b). More sophisticated analysis of this issue follows from approaches used by DiToro *et al* [this volume] and Fialko and Khazan [2005].

The characteristic distance also decreases with normal stress; there are complications, again related to extrusion of wear and melt in the unconfined tests. *DiToro et al* [this volume] report weakening distances of a few meters at normal stresses of 5 to 20 MPa whereas prior studies at 1.6 MPa have weakening over many tens of meters [*Hirose and Shimamoto, 2005*]. The difference is in part due to the addition of metal confining rings by *DiToro et al* [this volume]. Still, melt extrudes from the semi-confined fault at an approximately constant rate that increases with normal stress. *DiToro et al.* [this volume] argue that given a particular sliding velocity and a gradually decreasing melt production rate, since the extrusion rate increases with normal stress, the melt thickness decreases with normal stress. The time to get to steady state thickness decreases with normal stress, and the weakening distance is the product of the slip rate and weakening time [See Figure 4 in *DiToro et al.*, this volume]; their extrapolation to seismogenic depths predicts slip weakening distances on the order of tenths of meters at the base of the seismogenic zone.

*6.3.4 Dynamic strength recovery.* Although experiments have not investigated slip arrest carefully, anecdotal evidence is consistent with dynamic strength recovery contributing to arrest. In bulk melting experiments, once the clutch is disengaged, continued slip due to inertia is abruptly terminated due to melt solidification [*Hirose and Shimamoto, 2005*]. Noting the difficulties in interpreting arrest in stick-slip experiments (section 5), dynamic strength recovery is consistent also with inferences made in triaxial tests by *Koizumi et al.* [2004].

Melt is viscous and strongly rate strengthening ( $\tau \propto \eta V$ ) but also temperature weakening ( $\tau \propto \exp(1/T)$ ) through the strong dependence of viscosity on temperature. So, there are complicated non-linear interactions between strength, slip rate and temperature. Strength recovery would require that the increase in melt strength due to cooling exceeds the reduction in strength due to the reduction in slip speed during deceleration. While experiments are complicated by the roles of inertia and melt extrusion, arrest requires rapid cooling with respect to the duration of the event [also see *Fialko and Khazan, 2005*]. The conduction time constant is  $t = w^2/16\alpha$  [*Lachenbruch, 1980*], where  $\alpha$  is the thermal diffusivity. For lab tests with  $w = 0.12$  mm [*Hirose and Shimamoto, 2005*],  $t = 0.9$  ms and arrest is plausible. Some unpublished experiments are consistent with rapid strength changes associated with temperature fluctuation [*DiToro, private communication, 2006*]. Many natural pseudotachylites are 10 to 100 or more times thicker, making self-arrest less likely for the largest earthquakes, unless there are other mitigating factors. Based

on the preliminary data melting should produce large dynamic stress drops with relatively low fracture energy. Efficiency is unknown at present.

## CONCLUSIONS

It is generally accepted that stress drop  $\Delta\tau$  is independent of moment over the entire observable magnitude range [*Aki, 1967; Kanamori and Anderson, 1975; Hanks, 1977*] and typically a few megapascals. Some controversial observations suggest that apparent stress  $\tau_a$  increases by orders of magnitude from the smallest to the largest earthquakes requiring that efficiency  $\tau_a/\Delta\tau$  to increase by orders of magnitude with earthquake size. At present such systematic increases in efficiency are not observed. Typical efficiencies are in the range of 0.1 to 0.3. However, both higher and lower efficiency earthquakes are observed as are much larger and much smaller than typical static stress drops. Perhaps the wide range of source properties represent a range of different source physics. To distinguish changes in source physics with earthquake magnitude requires consideration of changes in both the static stress drop and efficiency.

In this context, laboratory observations of four mechanisms are adequate to estimate source properties. Conventional friction produces small stress drops and typical efficiencies, thus it can naturally explain source properties of typical seismic observations but not size-scaling of apparent stress. Unexpected weakening, attributed to silica gel produces large stress drops and typical efficiencies. This is not a likely mechanism to produce typical earthquake stress drops but could be involved in exceptional events. Flash melting will produce high efficiency events and therefore is not a likely mechanism for typical earthquake source properties. Dynamic stress drops are very large and on-fault effective shear fracture energies would be negligible for large events. Similar to flash melting, bulk melting will produce large dynamic stress drops. Not enough is known at present to estimate efficiency; the effective shear fracture energy for large earthquakes would be relatively small.

*Acknowledgements:* R. Abercrombie, J. Andrews, R. Archuleta, J. Dieterich, G. DiToro, K. Fischer, D. Forsyth, D. Goldsby, T. Hanks, B. Kilgore, D. Lockner, A. McGarr, J. Rice, P. Spudich, T. Tullis, J. Spray, A. Venkataraman, B. Walter, J. D. Weeks, and T.-f. Wong. Figures and explanations of experimental results were provided for the Chapman conference and this review by T. Shimamoto, V. Prakesh, D. Goldsby, T. Tullis, and G. DiToro. The paper was improved in response to comments by A. McGarr, J. Fletcher, A. Tsutsumi, an anonymous reviewer, and the associated editor G. DiToro. Thanks to the conference organizers, the editors, and AGU's book publication staff.

## REFERENCES

- Abercrombie, R. E., and J. R. Rice, Can observations of earthquake scaling constrain slip weakening?, *Geophysical Journal International*, 162, 406–424, 2005.
- Aki, K., Scaling law of seismic spectrum, *Bull. Seism. Soc. Am.*, 72, 1217–1231, 1967.
- Andrews, D. J., Rupture propagation with finite stress in anti-plane strain, *J. Geophys. Res.* 18, 3575–3582, 1976
- Andrews, D. J., Dynamic plane-strain shear rupture with a slip-weakening friction law calculated by a boundary integral method, *Bull. Seismol. Soc. Am.*, 75, 1–21, 1985.
- Andrews, D. J., Rupture dynamics with energy loss outside the slip zone, *J. Geophys. Res.*, 110, 14pp., 2005.
- Beeler, N. M., Stress drop with constant, scale independent seismic efficiency and overshoot, *Geophys. Res. Lett.*, 28, 3353–3356, 2001.
- Beeler, N. M., T.-f. Wong and S. H. Hickman, On the expected relationships among apparent stress, static stress drop, effective shear fracture energy and efficiency, *Bull. Seismol. Soc. Am.*, 93, 1381–1389, 2003.
- Beeler, N. M., T. E. Tullis, and D. L. Goldsby, Constitutive relationships and physical basis of fault strength due to flash-heating, submitted to *Journal of Geophysical Research*, 2006.
- Brace, W. F., and J. D. Byerlee, Stick slip as a mechanism for earthquakes, *Science*, 153, 990–992, 1966.
- Brown S. R., and C. H. Scholz, The closure of random elastic surfaces in contact, *J. Geophys. Res.*, 90, 5531–5545, 1985.
- Brune, J. N., Tectonic stress and the spectra of seismic shear waves from earthquakes, *J. Geophys. Res.*, 75, 4997–5009, 1970.
- Byerlee, J. D., The mechanics of stick-slip, *Tectonophysics*, 9, 475–486, 1970
- Byerlee, J. D., Friction of rocks, *Pure and Appl. Geophys.*, 116, 615–626, 1978
- Chester, J. S., Chester, F. M., Kronenberg, A. K., Fracture surface energy of the Punchbowl Fault, San Andreas system, *Nature*, 437, 133–135, 2005.
- Cocco, M. P., Spudich, and E. Tinti, On the mechanical work absorbed on faults during earthquake ruptures, in *Radiated energy and the physics of earthquakes*, AGU Monograph, eds Abercrombie, McGarr, Kanamori, and DiToro, 2006 .
- Cowie, P. A., and C. H. Scholz, Physical explanation for the displacement-length relationship of faults using a post-yield fracture mechanics model, *J. Struct. Geol.*, 14, 1133–1148, 1992.
- Dieterich, J. H., Time-dependent friction and the mechanics of stick slip, *Pure Appl. Geophys.*, 116, 790–806, 1978b.
- Dieterich, J. H., Modeling of rock friction 1. Experimental results and constitutive equations, *J. Geophys. Res.*, 84, 2161–2168, 1979.
- Dieterich, J. H. and B. D. Kilgore, Imaging surface contacts: power law contact distributions and contact stresses in quartz, calcite, glass and acrylic plastic, *Tectonophysics*, 256, 219–239, 1996.
- DiToro, G., D. L. Goldsby and T. E. Tullis, Friction falls towards zero in quartz rock as slip velocity approaches seismic rates, *Nature*, 47, 436–439, 2004.
- DiToro, G. S. Nielsen, and G. Pennacchioni, Earthquake rupture dynamics frozen in exhumed ancient faults, *Nature*, 436, 1009–1012, 2005.
- DiToro, G. T. Hirose, S. Nielsen, and T. Shimamoto, Relating high-velocity rock friction experiments to coseismic slip, this volume, 2006.
- Dugdale, D. S., Yielding of steel sheets containing slits, *J. Mech. Phys. Solids*, 8, 100–104, 1960.
- Fialko, Y. and Y. Khazan, Fusion by earthquake fault friction: Stick or slip?, *J. Geophys. Res.*, 110, doi:10.1029/2005JB003869, 2005.
- Friedman, M., J. Handin, and G. Alani, Fracture surface energy of rocks, *Int. J. Rock Mech. Mining Sci.*, 9, 757–766, 1972.
- Goldsby, D. L., and T. E. Tullis, Low frictional strength of quartz rocks at subseismic slip rates, *Geophys. Res. Lett.*, 29, 4 pp, 2002.
- Griffith, A. A., The phenomena of rupture and flow in solids, *Philos. Trans. R. Soc. London Ser. A* 221, 163–198, 1920.
- Gu, Y., and T.-f. Wong, Development of shear localization in simulated quartz gouge: effect of cumulative slip and grain size, *Pure & Appl. Geophys.*, 143, 388–423, 1994
- Gutteri, P., and P. Spudich, What can strong motion data tell us about slip-weakening fault friction laws, *Bull. Seismol. Soc. Am.*, 90, 98–116, 2000.
- Hanks, T. C., Earthquake stress drops, ambient tectonic stresses, and stresses that drive plate motions, *Pure Appl. Geophys.*, 115, 441–458, 1977.
- Heaton, T. H., Evidence for and implications of self-healing pulses of slip in earthquake rupture, *Phys. of Earth and Planetary Interiors*, 64, 1–20, 1990.
- Hirose, T. and T. Shimamoto, Fractal dimension of molten surfaces as a possible parameter to infer the slip-weakening distance of faults from natural pseudotachylytes, *J. Struct. Geol.*, 25, 1569–1574, 2003.
- Hirose, T. and T. Shimamoto, Growth of molten zone as a mechanism of slip weakening of simulated faults in gabbro during frictional melting, *J. Geophys. Res.*, 110, 2005.
- Husseini, M. I., and M. J. Randall, Rupture velocity and radiation efficiency, *Bull. Seismol. Soc. Am.*, 66, 1173–1187, 1976.
- Husseini, M. I., Energy balance for motion along a fault, *Geophys. J. Astr. Soc.*, 49, 699–714, 1977
- Ida, Y., Cohesive force across the tip of a longitudinal shear crack and Griffith's specific surface energy, *J. Geophys. Res.*, 77, 3796–3805, 1972.
- Ida, Y., The maximum acceleration of seismic ground motion, *Bull. Seismol. Soc. Am.* 63, 959–968, 1973.
- Ide, S., and G. C. Beroza, Does apparent stress vary with earthquake size?, *Geophys. Res. Lett.*, 28, 3349–3352, 2001.
- Ide, S., G. C. Beroza, S. G. Prejean, and W. L. Ellsworth, Earthquake scaling down to M1 observed at 2 km depth in the Long Valley Caldera, California, submitted to the *J. Geophys. Res.* 2002.
- Johnson, T., F. T. Wu, and C. H. Scholz, Source parameters for stick-slip and for earthquakes, *Science*, 179, 278, 1973
- Johnson, T. and C. Scholz, Dynamic properties of stick-slip friction of rock, *J. Geophys. Res.*, 81, 881–888, 1976.
- Kanamori, H., and T. H. Heaton, Microscopic and macroscopic physics of earthquakes, in *Geocomplexity and the physics of earthquakes*, *Geophys. Monogr. Ser.*, vol. 120, edited by J. Rundle, D. L. Turcotte, and W. Klein, pp. 147–155, AGU, Washington, D.C., 2000.
- Kanamori, H., E. Hauksson, L. K. Hutton, and L. M. Jones, Determination of earthquake energy release and  $M_L$  using terrascopes, *Bull. Seism. Soc. Am.*, 83, 330–346, 1993.
- Koizumi, Y., K. Otsuki, A. Takeuchi, and H. Nagahama, Frictional melting can terminate seismic slips, experimental results of stick-slips, *Geophys. Res. Lett.*, 31, 4pp., 2004.
- Kostrov, B. V., and S. Das, *Principles of earthquake source mechanics*, Cambridge University Press, 286 pp., 1988.
- Lachenbruch, A. H., Frictional heating, fluid pressure, and the resistance to fault motion, *J. Geophys. Res.*, 85, 6097–6112, 1980.
- Lin, A., and T. Shimamoto, Selective melting process as inferred from experimentally generated pseudotachylytes, *J. Asian Earth Sci.*, 16, 533–545, 1998.
- Lockner, D. A., P. G. Okubo, and J. H. Dieterich, Containment of stick-slip failures on a simulated fault by pore fluid injection, *Geophys. Res. Lett.*, 9, 801–804, 1982.

- Lockner, D. A., and P. G. Okubo, Measurements of frictional heating in granite, *J. Geophys. Res.*, *88*, 4313-4320, 1983.
- Lockner, D. A., and J. D. Byerlee, Fault growth and acoustic emissions in confined granite, *J. Appl. Mech. Rev.*, *45*, S165-S173, 1992.
- Madariaga, R., Dynamics of an expanding circular fault, *Bull. Seismol. Soc. Am.*, *66*, 639-666, 1976.
- Mayeda, K., and W. R. Walter, Moment, energy, stress drop, and source spectra of western United States earthquakes from regional coda envelopes, *J. Geophys. Res.*, *101*, 11,195-11,208, 1996.
- McGarr, A., Some comparisons between mining-induced and laboratory earthquakes, *Pure Appl. Geophys.*, *142*, 467-489, 1994.
- McGarr, A., On relating apparent stress to the stress causing earthquake fault slip, *J. Geophys. Res.*, *104*, 3003-3011, 1999.
- McGarr, A., and J. Fletcher, Maximum slip in earthquake fault zones, apparent stress, and stick-slip friction, *Bull. Seismol. Soc. Am.*, *93*, 2355-2362, 2003.
- McGarr, A., J. Fletcher, and N. M. Beeler, Attempting to bridge the gap between laboratory and seismic estimates of fracture energy, *Geophys. Res. Lett.*, *31*, 4pp, 2004.
- McKenzie, D., and J. N. Brune, Melting on fault planes during large earthquakes, *Geophys. J. R. Astr. Soc.*, *29*, 65-78, 1972.
- Ohnaka, M., Y. Kuwahara, K. Yamamoto, and T. Hirasawa, Dynamic breakdown processes and the generating mechanism for high-frequency elastic radiation during stick-slip instabilities, in *Earthquake Source Mechanics, Geophys. Monograph*, edited by S. Das, J. Boatwright, and C. H. Scholz, Amer. Geophys. Union, Washington, 13-24, 1986.
- Okubo, P. G., and J. H. Dieterich, Fracture energy of stick-slip events in a large scale biaxial experiment, *Geophys. Res. Lett.*, *8*, 887-890, 1981.
- Okubo, P. G., and J. H. Dieterich, Effects of physical fault properties on frictional instabilities produced on simulated faults, *J. Geophys. Res.*, *89*, 887-890, 1984.
- Orowan, E., Mechanism of seismic faulting in rock deformation, *Geol. Soc. Am. Mem.*, *79*, 323-345, 1960.
- Palmer, A. C. and J. R. Rice The growth of slip surfaces in the progressive failure of over-consolidated clay, *Proc. Roy. Soc. Lond.* A332, 527-548, 1973.
- Paterson, M. S. and T.-f. Wong, *Experimental rock deformation- The Brittle field*, Springer-Verlag, 347 pp, 2005.
- Perrin, G., J. R. Rice and G. Zheng, "Self-healing slip pulse on a frictional surface", *Journal of the Mechanics and Physics of Solids*, *43*, 1461-1495, 1995.
- Power, W. L., T. E. Tullis, S. R. Brown, G. N. Boitnott, and C. H. Scholz, Roughness of natural fault surfaces, *Geophys. Res. Lett.*, *14*, 29-32, 1987.
- Power, W. L., T. E. Tullis, and J. D. Weeks, Roughness and wear during brittle faulting, *J. Geophys. Res.*, *93*, 15,268-15,278, 1988.
- Randall, M. J., Stress drop and the ratio of seismic energy to moment, *J. Geophys. Res.*, *77*, 969-970, 1972.
- Rempel, A., The effects of flash-weakening and damage on the evolution of fault strength and temperature, this volume, 2006.
- Rice, J. R., The mechanics of earthquake rupture, in *Physics of the Earth's interior (Proceedings of the International School of Physics "Enrico Fermi", course 78, 1979)*, ed. by A. M. Dziwonski and E. Boschi, Italian Physical Society, North Holland Publ. Co., 555-649, 1980.
- Rice, J. R., Spatio-temporal complexity of slip on a fault, *J. Geophys. Res.*, *98*, 9885-9907, 1993.
- Rice, J. R., Heating and weakening of faults during earthquake slip, *Journal of Geophysical Research*, in press, 2006.
- Rice, J. R., Flash heating at asperity contacts and rate-dependent friction, *EOS Trans. Am. Geophys. Un.*, *80*, F681, 1999.
- Rice, J. R., and S. T. Tse, Dynamic motion of a single degree of freedom system following a rate and state dependent friction law, *J. Geophys. Res.*, *91*, 521-530, 1986.
- Ruina, A. L., Slip instability and state variable friction laws, *J. Geophys. Res.*, *88*, 10,359-10,370, 1983.
- Savage J. C., and M. D. Wood, the relation between apparent stress and stress drop, *Bull. Seismol. Soc. Am.*, *61*, 1381-1388, 1971.
- Scholz, C. H. and J. T. Engelder, The role of asperity indentation and ploughing in rock friction, I, Asperity creep and stick-slip, *Int. J. Rock Mech. Sci. Geomech. Abstr.*, *13*, 149-154, 1976.
- Scholz, C. H., and C. A. Aviles, The fractal geometry of faults and faulting, in *Earthquake Source Mechanics, Geophys. Monogr. Ser.*, vol. 3, edited by S. Das, J. Boatwright, and C. H. Scholz, pp. 147-155, AGU, Washington, D.C., 1986.
- Scholz, C. H., Wear and gouge formation in brittle faulting, *Geology*, *15*, 493-495, 1987.
- Scholz, C. H., The critical slip distance for seismic faulting, *Nature*, *336*, 761-763, 1988.
- Shaw, B. E., Far-field radiated energy scaling in elastodynamic earthquake fault models, *Bulletin of the Seismological Society of America*, *88*, 1457-1465, 1998.
- Shimamoto, T., J. Handin, and J. M. Logan, Specimen-apparatus interaction during stick-slip in a triaxial compression machine: a decoupled two-degree of freedom model, *Tectonophys.*, *67*, 175-205, 1980.
- Shimamoto, T. and A. Tsutsumi, A new rotary-shear high-speed frictional testing machine: its basic design and scope of research (in Japanese with English Abstract), *J. Tectonic Res. Group of Japan*, *39*, 65-78, 1994.
- Sibson, R., Generation of pseudotachylite by ancient seismic faulting, *Geophys. J. R. Astr. Soc.*, *43*, 775-794, 1975.
- Spray, J., Artificial generation of pseudotachylite using a friction welding apparatus: simulation of melting on a fault plane, *J. Struct. Geol.*, *9*, 49-60, 1987.
- Spray, J., Generation and crystallization of an amphibolite shear melt: An investigation using a radial friction welding apparatus, *Contrib. Mineral. Petrol.*, *99*, 464-475, 1988.
- Spray, J., Viscosity determinations of some frictionally generated silicate melts: Implications for fault zone rheology at high strain rates, *J. Geophys. Res.*, *98*, 8053-8068, 1993.
- Summers, R., and J. Byerlee, Summary of results of frictional sliding studies, at confining pressures up to 6.98 kb, in selected rock materials, *U.S. Geological Survey, Open File Report 77-142*, 129, 1977.
- Tsutsumi, A., and T. Shimamoto, High-velocity frictional properties of gabbro, *Geophys. Res. Lett.*, *24*, 699-702, 1997.
- Venkataraman, A., and H. Kanamori, Observational constraints on the fracture energy of subduction zone earthquakes, *J. Geophys. Res.*, *109*, 26 pp., 2004.
- Wilson, B., T. Dewers, Z. Reches and J. Brune, Particle size and energetics of gouge from earthquake rupture zones, *Nature*, *434*, 749-752, 2005.
- Wong, T.-f., Shear fracture energy of Westerly granite from post-failure behavior, *J. Geophys. Res.*, *87*, 990-1000, 1982.
- Wong, T.-f., On the normal stress dependence of the shear fracture energy, in *Earthquake Source Mechanics, Geophys. Monogr. Ser.*, Vol. 37, edited by S. Das et al., pp. 1-11, AGU, Washington, D.C., 1986.
- Yund, R. A., Blanpied, M. L., Weeks, J. D., and Tullis, T. E., Observation and interpretation of microstructures in experimental fault gouges, *J. Geophys. Res.*, *95*, 15589-15602, 1990.
- Zheng, G., and J. R. Rice, Conditions under which velocity-weakening friction allows a self-healing versus a cracklike mode of rupture, *Bull. Seismol. Soc. of Am.*, *88*, 1466-1483, 1998.

